

NOTICE WARNING CONCERNING COPYRIGHT RESTRICTIONS:

The copyright law of the United States (title 17, U.S. Code) governs the making of photocopies or other reproductions of copyrighted material. Any copying of this document without permission of its author may be prohibited by law.

**Thermal Design of Wearable Computes: Application
to the Navigator 2, Thermal Management Devices,
and Embedded Electronics**

Eric Egan and Cristina Amon

EDRC 24-123-95

Thermal Design of Wearable Computers: Application to the Navigator2.
Thermal Management Devices... and Embedded Electronics

Eric Egan and Cristina Amon
November 16, 1995

This work has been supported by the Engineering Design Research Center, an Engineering Research Center of the National Science Foundation, under Grant No. EEC-8943164

Abstract

A portable computer that can be worn on the body produces unique design constraints. The wearable computer must be rugged, lightweight, small, and power-efficient. The most recently-developed wearable computer is the Navigator2 which will be used as a computerized maintenance manual with the capacity of speech recognition. Its thermal management develops concurrently with the overall design of the Navigator2.

The first stage of the thermal design is to select the type of cooling arrangement that is needed. With a completely closed housing and an anticipated power level of approximately 10W, it is decided early in the thermal management to use conduction to transfer the heat to the outer casing where it is then dissipated through natural convection.

In the second stage of the thermal design, the thermal contact between the aluminum heat spreader (used to conduct heat to the outer casing) and the electronics is optimized. The liquid heat sink (LHS) by 3M, Inc. and the Gap Pad by the Bergquist Company are two thermal interfaces that were tested. The LHS is a plastic pouch filled with fluorinert liquid that produces an isothermal platform. On the other hand, the Gap Pad is a conductive elastomer. In experiments conducted on these devices, the Gap Pad consistently yielded a smaller temperature rise from the electronics to the surrounding air and is chosen as the thermal interface.

The third stage consists of numerical simulations modelling the conduction of heat of the Navigator2 using natural convection as the boundary conditions. This conduction-only model approximates the temperatures that are expected in the Navigator2 before it is manufactured and predicts that an area of 150 in² of aluminum needs to be exposed to the ambient air to adequately cool the electronics.

Another aspect of the thermal design of wearable computers is that of embedded electronics. Because a portable computer worn on the body imposes unique design constraints, it has been postulated that embedding the electronics in a plastic substrate could aid the conduction heat transfer. By depositing the plastic material over the electronics, all air gaps are practically eliminated, leaving a nearly perfect avenue for the heat to transfer into the substrate. Thus, the plastic aids the heat spreader in removing the heat, making it easier to

minimize the maximum temperature within the wearable computer—the goal of the thermal design.

Three main parameters are involved in the thermal design of embedded electronics: the heat spreader, air channels, and substrate material. The heat spreader consists of an aluminum plate which has good thermal contact with the heat-producing elements. The heat spreader then extends out of the substrate into the ambient air where heat is removed by natural convection. Air channels through the substrate aid the process of natural convection by exposing more of the heat spreader to the ambient air. Various polymer composites were investigated to determine the effect of the conductivity of the polymer composite upon the overall heat transfer. The conductivity of the polymer composite can be changed by varying the amount, type, grain size, and orientation of the conductive filler that is blended with the epoxy.

1. Introduction

The goal of the thermal design for any computer is to determine an efficient means of cooling the computer's electronic components such that the operating temperature of each component does not exceed manufacturer- suggested limits. To meet this goal, the power and size of the computer, as well as its environment, must be taken into account to achieve an efficient thermal design. The focus of this research involves the thermal design of computers that are portable, lightweight, and rugged. These computers are meant to be worn and used on the body and are known as wearable computers.

In addition to the thermal aspects of wearable computer design, it is necessary to coordinate with other design criteria. A thermal designer cannot arbitrarily select the size, shape, and placement of heat spreaders to conduct heat away from the heat-generating electronics. Industrial design considerations such as the weight, size, and appearance of the wearable computer affect, for example, the size, shape, and placement of the heat sink (typically a metallic surface where heat is transferred to the air stream by convection) on the outer surface. Furthermore, power consumption and placement of the heat-producing elements are typically a result of decisions made by the electronics team. This type of design procedure involves many different areas of specialization from electronics to thermal design to industrial design requiring good interdisciplinary design skills and cooperation. As the different phases of design from other disciplines mature, the thermal design must adjust accordingly. Concurrent design at each stage of the process is the only way to assure that the thermal design meets the requirements of the changing wearable computer. Concurrent thermal design involves the use of numerical simulations and analytical approximations to predict at each stage the thermal limitations of the design (S. Finger *et al*, 1994). Therefore, a good thermal design is one that keeps pace with all of the developments in the overall design of the wearable computer.

Forced air convection is employed in most computer thermal designs. In the thermal design of wearable computers, however, there are more constraints than the average laptop computer. Wearable computers need to be small, lightweight, and ergonomic and often must operate in wet and dirty environments for applications such as those of the marines. This renders air ventilation slots on the outer case infeasible and the use of fans impractical. Furthermore, because wearable computers are powered from a battery pack, power usage must be minimized. Therefore, power-consuming cooling devices like thermoelectric modules are

not typically the best solution. Hence, removal of heat simply by conduction becomes all the more attractive since it consumes no power and needs no moving parts. The thermal design of wearable computers optimizes the conduction of heat from the electronic elements to the outer casing as well as its removal by natural convection.

Because conduction is a preferable mode of heat transfer for wearable computers, it has been postulated that embedding the electronics in a polymer-filler composite substrate could aid the design of wearable computers in several ways. First, by surrounding the electronics within a protective region of plastic, the design would be more rugged. Second, the embedding process is more economical since the plastic material can be poured into the mold containing the electronic board(s). Lastly, embedding the electronics definitely aids in the removal of heat when the substrate has a sufficiently high conductivity. By eliminating nearly all the air gaps, an avenue is made for the heat to transfer away from the electronics through the substrate. Heat transfer into the substrate reduces the reliance upon the heat spreader. Also, a layer of highly conductive substrate can be used to enhance the thermal performance making it easier to minimize the maximum temperature within the wearable computer-the goal of the thermal design.

We investigate various ways to remove heat from the embedded electronics by testing several parameters. These include the use of heat spreaders and/or air channels as well as the type of substrate material. The heat spreader consists of an aluminum plate which is in good thermal contact with the heat-producing component. The heat spreader then extends out of the substrate into the ambient air where the heat is removed by natural convection. We cut air channels through the substrate to allow more surface area of the heat spreader to be in contact with the air improving the removal of heat with natural convection. Different materials are investigated to see the effect of material conductivity on the overall heat transfer.

Because the conductivity of the substrate material is very important for conduction, the value of the material conductivity must be ascertained with reasonably good accuracy. To this end, a carbon resistor is embedded in a plastic substrate. By comparing the results of the numerical simulation with those obtained from physical experiments, an estimate of the conductivity of the substrate is made. A more precise and easier experimental method using heat flux sensors has been developed as a better alternative for determining the conductivity of a given material.

2. Concurrent Thermal Engineering

In the process of designing a robust portable computer that is comfortably worn, highly functional, easily used, and very dependable, many disciplines are required to work in parallel with each contributing to the overall product: the wearable computer. For wearable computers, thermal design cannot be an afterthought. Communication with other disciplines is extremely important to produce the most advantageous thermal design that can satisfy not only the needs of the thermal constraints but the needs of the other disciplines as well. For example, the electrical engineering team must be informed from the outset that high power electronics not only inhibit battery life but also constitute an important thermal design issue. Industrial designs must also be addressed. For wearable computers, the outer casing must incorporate the heat sink to facilitate natural convection heat removal. The heat sink must not only satisfy thermal design but also aesthetic and ergonomic criteria as well. Therefore, because thermal design is highly dependent on, and constrained by, other disciplines, personal interaction with designers from other disciplines is necessary, demanding a cohesive design framework in which progress at all levels is performed concurrently.

Communication, however, is only one aspect of concurrent engineering. The thermal design must affect the design of the overall product at each stage of the design process, and much of the responsibility falls on the thermal designer. The tools of modern thermal engineering are analytical formulations, numerical simulations, and physical experimentation. As the design progresses, the thermal designer must employ those tools which are appropriate as the overall design matures to insure an adequate thermal solution.

2.1 Framework of Concurrent Thermal Engineering

With the application of wearable computers, the thermal design must be flexible and responsive to changes in the designs from the other disciplines. However, a certain systematic methods guide the thermal designer through the design process (Nigen and Amon, 1992) and consists of three stages. The first stage of the thermal design is to select the type of cooling arrangement that is needed. To do this, first the electronics must be specified with their appropriate layout and power levels. Then, a preliminary analytical estimation is made to determine how much heat is produced and how it should be dissipated.

In the second stage, the actual device(s) and the expected implementation are tested. The thermal management devices, used in addition to the aluminum heat spreader, include: thermal paste, thermally conductive adhesive, and various other thermal interfaces between the heat-producing components and the heat spreader. For testing these devices, a physical experiment is constructed to validate their application for the wearable computer. With increased knowledge from this stage, the actual device(s) can be selected to fulfill the demands of the first stage.

After the appropriate device(s) has been selected, the third stage, consisting mainly of numerical simulations, begins. In the numerical simulations, a conduction-only model of the wearable computer is usually adequate to gain a rough approximation of the temperature distribution throughout its domain. For a more accurate prediction of the temperature distribution, a conjugate conduction/convection simulation is made before the final prototype is constructed. The conjugate conduction/convection simulation solves the energy equation for both the fluid and solid domains. This simulation takes a substantial amount of time even with high speed, high capacity computational facilities and is, therefore, used only in the last stage of the thermal design.

2.2 An Application of Concurrent Thermal Engineering: the Navigator2

The Navigator2 is a wearable computer designed for the US Marines and Boeing Corporation to be used by both entities as a computerized maintenance manual. Some of its capabilities include global position sensing (GPS), speech recognition, radio and wireless LAN communication, and heads-up display. In the overall design, the electrical engineering group focuses on minimizing the number, size and power usage of the electronics. In the industrial design, smooth contours and small size are defining characteristics. The decisions made by the electrical engineering and industrial design teams strongly affects the thermal design.

In the first stage of the thermal design, it was anticipated by the electronics group that a power level of approximately 10 W would be needed. Furthermore, the use of forced air convection across the electronics was considered impractical because the Navigator2 is designed with a completely closed housing for rugged, wet, and dirty

conditions. Therefore, it was decided early in the design process that heat must be transferred by conduction to the outer casing and then be dissipated by natural convection. Because the air gap between the electronics and the heat spreader constitutes the largest thermal resistance that can be minimized in the conductive path to the outer casing, the focal point of the thermal design is the thermal contact between the electronics and the aluminum heat spreader.

In the second stage, two thermal interface devices are tested with a heat sink test bed (see Fig. 1 and 2). The two devices to be tested are the liquid heat sink (LHS) by 3M, Inc. and the Gap Pad by the Bergquist Company. The heat sink test bed consisted of eight 7805 voltage regulators which can produce between three and 20 watts of power. In these experiments, a Gap Pad of 0.125 inch thickness out-performed the LHS by some 25%, based on the overall temperature rise from the case of the voltage regulators to the surrounding air of the inside of the test bed. The LHS offers an isothermal platform from which to conduct the heat, but this characteristic was not considered important enough to overcome the implementation complexities required by the LHS such as the necessity of even pressure distribution along the LHS packet. Thus, the Gap Pad was chosen as the thermal interface between the electronics and the heat spreader.

The third stage of thermal development consists of numerical simulations conducted to obtain a detailed account of the approximate temperatures that could be expected throughout the structure of the Navigator2. The geometry of the model was simplified for the simulations, and the stagnant air inside the housing was modeled as a solid with the properties of air (Lee *et al*, 1994). Thus, the internal mode of heat transfer is conduction, while natural convection removes the heat on the outside of the housing. It was primarily through this model that an aluminum heat sink with an area of 150 in² needs to be exposed to the air on the outside to adequately cool the electronics well below the manufacture's limit.

3. Thermal Design of the Navigator2

The thermal development of the Navigator2 took the form of the three-stage design process outlined above. In concurrent thermal design, one of the main challenges is the lack of timely information from other disciplines. For example, the experimentation of the

thermal interface devices was conducted before the electronics were completely specified. Once the hardware was finalized, the numerical simulations were begun.

3.1 The Electronics of the Navigator2

The latest version of the Navigator2 has just one printed circuit board (PCB) with electrical components mounted on each side of the PCB. The expected power ratings of the major heat-producing components are documented in Table 1.

The other components of the Navigator2 are assumed not to produce much heat and are therefore neglected in the thermal analysis. Also, this is a list of the components used in the initial numerical simulations. However, the prototype of the Navigator2 has only two voltage regulators since the 78SR174HC voltage regulator has been replaced with a transistor. It should be noted that the Epson Card is a compact electronic, aluminum-cased package containing the microprocessor and its necessary accessories.

3.2 Power-Saving Features for the Navigator2

The electronic and software design teams made it a priority to reduce the power consumption of the Navigator2 so that battery life could be maximized and operating temperatures minimized.

The first design choice of the electronic team was the Viper Board, consisting of an Intel 33 MHz 486 microprocessor, 16 MB of Dynamic Ram, 1 MB of Erasable Programmable Memory (EPROM), and a VGA controller. Thermally, the major drawback of the Viper Board is its power consumption, rated at 7.5 W. The second design choice consisted of the Epson Card. This card has the same level of capabilities while producing significantly less power (4.5 W).

For the Epson Card, there are three levels of power savings that can be manipulated. The first is the CPU Standby Mode where the CPU clock stops, and the system goes non-operational. This mode occurs when there are no system events for a certain period of time which can be set as low as 4 seconds or up to 17 minutes. The Global Standby Mode occurs only after a certain period of time the system has been in

CPU Standby Mode. This time is set between 4 seconds and 36 hours. In this mode, almost all devices go into the standby state, further saving power. The final layer of power saving capability is provided by the Auto Suspend State. This state occurs only after a certain period of time has elapsed in Global Standby Mode. The timer can be set from 4 seconds to 36 hours, and in this state power is shut off for almost all devices.

The recommended time switches for all of the settings given by the Navigator2 Power Management Team and are listed in Table 2.

3.3 Thermal Design Experiments for the Navigator2

Using the heat sink test bed shown in Figure 1, a physical system modeling a generic wearable computer was created in which various heat spreaders and thermal interfaces could be tested. The heat sink test bed is made of a Rubbermaid container of the approximate size of the Navigator2. Its construction allows for near air-tight conditions simulating the mostly stagnant air found inside wearable computers. Eight 7805 voltage regulators simulate the heat-producing components of a wearable computer.

In all, seventeen experiments are conducted. Experiments are conducted at the 3.0 W, 5.0 W, and 8.0 W power levels, with and without heat spreaders, and with either the Gap Pad or the LHS as the thermal interface. Table 3 summarizes the aluminum heat spreaders that are used.

For each of the experiments, thermocouples measure the temperature at selected points. For the first 11 experiments, the thermocouple wire and heads were slightly bulky and introduced air gaps (thus enlarging the temperature rise measurements). In subsequent experiments, thermocouples specifically designed for surface temperature measurement are employed that are thinner, smaller, and have an adhesive backing providing good contact with the surface. Figure 3 shows the five locations in which the temperature data was taken. Table 4 presents the experimental data.

In the evaluation of this experimental data, the main component of interest is the overall temperature rise (T_i-5). This represents the temperature rise between the stagnant air inside the wearable computer to the highest heat-producing component. Because the Epson Card has a rated maximum operating temperature of 55°C and the stagnant air

inside the wearable computer could easily approach 35°C, the overall temperature rise of the Navigator2 should be kept below 20°C

In the first eleven experiments, the effectiveness of the thermal interfaces are evaluated. Experiments 4 & 5, 8 & 9, and 10 & 11 find which interface gives the smallest overall Ti-5 and local (Ti-3) temperature rises when used with a heat spreader. The temperature rises are presented in Table 5.

The table shows that the Gap Pad yields a local temperature rise consistently less than that of the LHS by several degrees Celsius. Thus, the Gap Pad is chosen as the thermal interface between the heat-producing components and the heat spreader.

Once the thermal interface is chosen, different power levels, heat spreaders, and types of Gap Pad are explored in the next set of experiments. Experiments 12 through 17 used a thermocouple consisting of very fine wire made specifically for surface temperature measurements which adheres to the surface with an adhesive tape backing; therefore, their results cannot be directly compared with those from the earlier experiments. Hence, more accurate measurements are obtained in experiments 12 through 17 than in the previous experiments.

In addition to thermal interface materials, three different heat spreaders are used for these experiments. As the surface area of the heat spreader exposed to air is enlarged by a factor of three, experiments 13 and 14 show that the overall temperature rise falls by 3.8 degrees, a change of 13%. In experiments 15 and 16, different thicknesses are used for the heat spreaders. Doubling the thickness from 0.0625 inches to 0.125 inches causes the overall temperature rise to fall by three degrees, with the heat spreader temperature drop simply being cut by a factor of two (a 14.9°C drop was reduced to 7.7°C). Thus, increasing the thickness and the surface area of the heat spreader produces a significant lowering of the overall temperature rise.

In experiments 15 through 17, an 8.0 W power level was used to obtain more realistic data for the Navigator2. Increasing the power from 3.0 W to 8.0 W (an increase of 267%) results in an 188% increase in the overall temperature rise from experiment 14 to 15. This shows that as the temperature rises, the convective thermal resistance from the heat spreader to the air reduces, and the heat spreader becomes more efficient at dissipating heat.

The benefits of using a thinner Gap Pad with adhesive on the glass-fiber reinforced side that is in contact with the heat spreader are two fold. First, reducing the thickness by a factor of two reduces the temperature difference through the Gap Pad by that same factor. Second, the Gap Pad is in excellent contact with the electronics due to the conformable nature of the Gap Pad material, but the glass-fiber reinforced layer has less contact with the heat spreader than the side in contact with the electronics. The adhesive backing helps the Gap Pad to adhere better to the heat spreader. The combined effect of the Gap Pad with the reduced thickness and the adhesive backing is shown by comparing the local temperature rise ($T_i - T_3$) from experiments 16 and 17. The local temperature rise fell from 24.4 °C to 16.5 °C, a reduction of 32%, and the overall temperature rise is reduced by 4.3 °C. Therefore, using as thin Gap Pad as possible with adhesive backing produces significant results.

Thus, the heat sink test bed experiments reveal several important findings. First, although the Gap Pad cannot boast an isothermal temperature distribution like the LHS, the Gap Pad consistently out-performs the LHS. Second, adding surface area and thickness to the heat spreaders as well as using a thin Gap Pad with the pressure sensitive adhesive yields the best results.

3.3 Numerical Simulations for the Navigator2

To obtain an accurate estimation of the temperature distribution within the Navigator2, numerical simulations were performed using version 2.8 of Nekton. Two meshes are generated with simplified geometry and estimated material properties. Figure 4 shows the second mesh. The material properties of the two meshes is shown in Table 3. The Navigator2 will be have a complex, rounded shape. The meshes, although rectangular, are of the same approximate surface area and volume of the Navigator2. In the mesh-generation process, the Navigator2 is represented by a series of layers built up on top of one another. Each layer is composed of blocks representing different components and segments. Such simplified geometry permits the shape to look like a shoebox but still can accurately predict the thermal behavior of the Navigator2. Another simplification is that only the major heat-producing elements are modeled, namely the three voltage regulators and the Epson Card.

The difference between the first mesh and the second is the thickness of the aluminum subframe, the heat spreader, and the plastic housing (see Fig. 5 for a cross-sectional view of one of the layers and Fig. 6 for the vertical cross-sectional view). The heat spreader, the aluminum subframe, and the housing have the same thickness in each mesh. The first mesh used a thickness of 0.0625 inches; the second mesh used a thickness of 0.125 inches. For both meshes, a thickness of 0.0625 inches is used for the Gap Pad.

The Gap Pad is given a reduced conductivity in an attempt to model the effect of contact resistance between the Gap Pad and the electronics components as well as between the Gap Pad and the heat spreader. A lumped analysis is undertaken to estimate the conductivity for the Gap Pad-contact resistance model. For the thicknesses and conductivities involved, a conductivity of approximately 1/3 the original conductivity of the Gap Pad effectively models potential problems with air voids. A more detailed analysis was done concerning the improvement of the conductive heat transfer from the electronics to the heat spreader when using Gap Pad as opposed to no thermal interface. It is determined that conduction of heat from the electronics to the heat spreader is roughly twice as efficient when using Gap Pad, compared to no interface at all.

Table 6 shows the results of the simulations for both the first mesh and the second mesh. The parameters that were varied are the heat transfer coefficient along the sides, the heat spreader area exposed to the air, the conductivity of the metal used for the heat spreader and the subframe, and the conductivity used for the Gap Pad.

Because mesh generation is time consuming, the actual mesh was not altered to enlarge the heat spreader area. Instead the effect of enlarging the heat spreader was simulated by increasing the convection coefficient used for that area. Therefore, when it is reported that the exposed heat spreader area is doubled, in actuality, it is the convection coefficient that is doubled (since convective thermal resistance is proportional to $1/hA$, where h is the convection coefficient and A is the exposed heat spreader area). This method of simulation, however, does not model the added thermal resistance due to conduction through the larger surface area of the heat spreader, causing the resulting overall temperature rise to be slightly less than what would actually occur.

In simulations (a) through (e), it becomes apparent that regardless of the conductivity used for the Gap Pad or the metal, the temperature begins to fall in significant amounts only when the heat spreader surface area exposed to air is enlarged.

The second mesh was constructed to test the thermal effect of doubling the thickness of the plastic housing, the metal subframe, and the heat spreader. With this mesh, a more realistic boundary condition is used for the sides and bottom of the Navigator2. Since the Navigator 2 will have its bottom and sides encapsulated in the harness, which keeps it secured to the user's back, a much smaller convection coefficient is used than for the top which is exposed to the air. An insulated boundary condition is inappropriate since some heat will undoubtedly escape from the sides and bottom of the Navigator2. However, since it is difficult to ascertain exactly how much heat will escape from the encapsulated areas, the convection coefficient was simply lowered from $5 \text{ W/m}^2 \text{ K}$ to $1 \text{ W/m}^2 \text{ K}$.

In simulations (g) through (p), the exposed heat spreader area is again found to be the main factor causing the temperature to fall as the area is enlarged. There are, however, cases where a smaller temperature is the result of the conductivity value and not the exposed heat spreader area. For example, simulation (k) is lower in temperature than simulation (j) even though simulation (k) has 17% less heat spreader area. The reason for the better results of simulation (k) is its Gap Pad conductivity, where the contact resistance is assumed to be zero. From simulation (l) to (m), even though the exposed heat spreader area is reduced by 14%, the temperature is reduced by $0.2 \text{ }^\circ\text{C}$ since the conductivity of the subframe and heat spreader metal is doubled. Therefore, changing to a more conductive metal or reducing the contact resistance of the Gap Pad can make a positive impact in the thermal performance, but ultimately the amount of exposed surface area of the heat spreader determines the heat that can be dissipated in the conjugate conduction-convection system.

Mainly, simulations (g) through (p) were used in the thermal design process since the Navigator2 will have primarily a 1/8 inch housing thickness. Simulation (m) is considered the most appropriate thermal model since the conductivity of the metal is that of aluminum, a moderate contact resistance for the interfaces of the Gap Pad is included, and the overall temperature rise is less than $20 \text{ }^\circ\text{C}$ over the ambient temperature ($25 \text{ }^\circ\text{C}$). Therefore, the thermal design of the Navigator2 calls for a conduction-convection heat transfer scheme employing 1/16 inch-thick Gap Pad with pressure sensitive adhesive as the thermal interface and 150 in^2 of exposed surface area of the 1/8 inch-thick aluminum heat spreader.

Recently, a more detailed mesh of the Navigator2 was made to portray its actual shape. The numerical simulations have not been completed, but Figure 7 displays its appearance.

3.4 Thermal Management Devices for Wearable Computers

In the thermal management of wearable computers, certain devices are commonly employed to efficiently remove heat from the heat-producing electronics and thus greatly improve the reliability and life expectancy of the product (Johnson, 1989). Thermal management devices vary greatly from the mode of heat transfer employed to remove the heat to the physical mechanism by which it functions. They differ in their size, weight, thermal efficiency, durability, cost, and their intended application.

3.4.1 Flat Plate Heat Sinks

Of the thermal management devices, flat plate heat sinks are among the most common devices used in the cooling of electronic components. Flat plate heat sinks are metallic strips that are placed in good contact with the electronic component via thermal grease or another thermal interface that insures good thermal contact. Heat from the component is transferred to the surroundings by the combined effects of natural convection and thermal radiation (Ahmad *et al*, 1994).

A recent systematic study on the implementation of flat heat sinks with surface coatings suggests that radiation can perform an important role in the heat transfer. Table 7 consists of data from two identical heat sinks dissipating the same amount of heat with the same boundary conditions.

The emissivity of the heat sinks is the only parameter that is changed. By increasing the emissivity by four fold, the surface coating (black, anodized) of the aluminum heat sink doubled the amount of heat drawn from the component to the heat sink by 8%, the temperature drop of the component was significant, 11.5 °C, representing a 19% decrease in the temperature rise of the component. Thus, flat heat sinks, when properly designed and installed, can offer a very good thermal solution.

3.4.2 Liquid Heat Sinks

The liquid heat sink (LHS), pioneered by 3M, Inc., is a relatively new device offering an enhanced thermal management cooling technique. The LHS consists of a flame-retardant plastic pouch that is filled with perfluorinated (Fluorinert) liquid. The conformable nature of the pouch allows the LHS to be pressed against uneven surfaces of the heat-producing board components. The heat is conducted from the components into the plastic pouch where the high rate of thermal expansion of the liquid produces efficient natural convection that transfers the heat to the other side of the bag where heat can be removed by a cold wall or finned heat sink (Remsburg, 1991).

The LHS developed by 3M, Inc. has intrinsic qualities that lend itself well to small computer systems. First, it is very thin (one-eighth of an inch). Second, its liquid characteristics give it the ability to provide the electronics with some shock absorption (from a drop test conducted on a computer disk drive: with the LHS, the maximum G force sustained was 50; without the LHS, the maximum G force was 60, indicating a slight cushioning effect with the LHS). Third, it can be used in conjunction with heat spreaders, finned heat sinks, or other devices depending on the urgency of the situation. Fourth, it can conform to geometrical irregularities. Finally, it adds thermal inertia to the system (it not only smoothes out the high spots in temperature but keeps the temperature from going through quick fluctuations, as well) (3M Inc., 1994).

The first application of the LHS was the NCR "Model 32/200", a desktop tower microcomputer whose circuit board produces 60 W. Through physical experiments in which the results of conventional, forced-air laminar flow are compared to those of the LHS-cooled circuit board, the LHS was found to be superior to the traditional air-cooled technique. Chip temperatures using the LHS were consistently below that of the forced-air cooling. Furthermore, the LHS produces an isothermal effect, averaging the temperature distribution across the components (Wall, 1989). Typical temperature variations across components cooled by forced-air convection can be as high as 30 °C; the LHS reduces this range to 8 °C.

3A3 Miniature Heat Pipes

One of the most effective ways of cooling electronic components is achieved through heat pipes. Heat pipes require no power to operate, have no moving parts, and produce no noise. The thermal mechanism of heat pipes lies in the phase change of the liquid within the heat pipe. Typically, heat will enter one end of the heat pipe, the evaporator region, and cause the liquid to evaporate. The gaseous fluid moves through the adiabatic section due to a pressure gradient and enters the condenser region. Once in the liquid phase, it travels back to the evaporator region either by gravity or capillary force (Sridhar *et al*, 1994). In this manner, the heat exits the liquid at the condenser section where typically a heat sink is employed to efficiently transport the heat to the surroundings.

Micro heat pipes etched onto the top of semiconductor chips have been found to act as an idealized heat spreader (Peterson, *et al*, 1992). Heat pipes of a triangular cross section on the order of 100 μm and 20 mm long provide an array of parallel heat pipes. The result is much reduced temperature gradients and more uniform heat fluxes. By placing heat sinks on the edges of the chips perpendicular to the plane of heat pipes and using only 1.35% of the surface area with the heat pipes, the maximum chip temperature was reduced by 40%.

3.4.4 Power-Consuming Thermal Management Devices

Other thermal management devices have been designed that are very effective at removing heat but need to be supplied with power to operate. Such devices are the liquid cold plate, heat sinks with built-in fans, and the thermoelectric module.

Liquid cold plates are finned passages usually made of aluminum or copper in which a low-pressure liquid circulates to remove liquid by convection from the heat producing components mounted on the cold plate. Using water, for example, to cool electronics is practical because it is an excellent transporter of heat. Its density is 800 times that of air, and its specific gravity is 1.0 as opposed to 0.24 for air, causing water to be much more efficient in carrying heat per unit volume (Soule, 1992). Cold plates can remove higher heat fluxes than traditional finned heat sinks thereby allowing components

to be placed closer together on circuit boards (Pei and Lawson, 1993). The disadvantage of cold plates is their weight to volume ratio and the required pumping power.

Heat sinks with built-in fans also require an input power but are lightweight and quite effective. These heat sinks have fans built inside them (Pei and Lawson, 1993) and offer a type of jet impingement cooling where the coolant jets of air directly impact the surface instead of flowing parallel to it. This breaks the boundary layer causing the heat transfer coefficient to be up to ten times higher than normal forced-convection ones (Remsburg, 1994).

One of the most interesting devices is the thermoelectric module (TEM). This is a solid-state, miniature refrigerator ranging in size from 3 mm to 50 mm laterally and from 3 mm to 6 mm vertically. TEM's are lightweight and noise-free. Furthermore, they can cool components below room temperature. TEM's operate by passing a current through metals of different type, thus, creating a temperature difference between the junctions. TEM's can also be stacked on top of one another to create higher temperature differentials (Sridhar era/, 1994).

4. Embedded Electronics

The unique engineering challenges of designing a wearable computer put many constraints on the thermal design. The framework of these constraints is formed by the network of needs that the wearable computer must satisfy. The wearable computer must be small, lightweight, and ergonomic in order to be worn on the body comfortably, yet it must be rugged and also be able to be splashed by water and allowed to get dirty; it is not being designed for an office environment. Furthermore, the power usage of the wearable computer must be kept to a minimum so as to extend its battery life. Within all of these constraints, the thermal design is to produce a reliable computer that will operate below the maximum operating temperature of each of its electronic components.

Because of these constraints, embedding the electronics within a substrate is a good option (Bujard, 1988). With this design, the mode of heat transfer within the wearable computer is conduction. Using metallic heat spreaders and the substrate itself, the heat is transferred to the outer casing where it is dissipated through natural air convection. This thermal design needs no battery power, has no moving parts, needs no air vents, and causes the wearable computer to be extremely rugged. It is for these reasons that embedding electronics within a polymer substrate is the focus of my research.

4.1 Numerical Technique

The numerical technique underlying the simulations to be discussed is called the spectral element method. The spectral element method is a hybrid of two powerful techniques: the finite element method and the spectral technique. From the finite element method, the spectral element method retains the advantages of geometric flexibility and sub-domain integral formulation, whereas it acquires the advantages of rapid convergence and high memory efficiency from the spectral technique (Nigen, 1994).

The spectral element method uses Lagrangian interpolants instead of trial functions, similar to finite element methods; however, unlike finite element methods, the Lagrangian interpolants are constructed from higher order orthogonal polynomials. For the orthogonal collocation technique employed, Gauss-Lobatto points are chosen corresponding to the roots of the selected polynomials which increases its accuracy.

The discretization of the spectral element method divides the domain into macro elements that are isoparametrically mapped to a local coordinate system. Each macro element is further numerically divided by internal collocation points. The number of collocation points to be used per element is controlled by the user. For the three-dimensional macro elements used in the simulations, a scheme of 5x5x5 collocation points was used for each macro element. It is at each of these collocation points where the temperature is calculated and the differential energy equation is exactly satisfied for the steady-state, conduction-only model.

4.2 Numerical Simulations

To gain more understanding of the thermal phenomena of embedded electronics, a model was constructed so that the various parameters that affect the heat transfer could be tested. This model consists of a geometric mesh using the Nekton v2.8 software. The mesh consisted of three dimensional macro elements modeling a 3.0x3.1x2.5 in³ embedded electronic artifact.

The artifact uses a polyurethane composite substrate where the polyurethane is mixed with a filler (either aluminum oxide or nylon powder). Inside the substrate, in the center of the artifact, an integrated switching voltage regulator (the 78ST305HC from Power Trends, Inc.) is used as the heat-producing element. The voltage regulator is attached to the cross-shaped, aluminum heat spreader by a thermal adhesive compound. Figure 8 shows the schematic representation of the physical model.

4.2.1 Embedded Voltage Regulator Mesh Design

Several meshes of the embedded voltage regulator "cube" were constructed. The first mesh to be constructed consisted of a heat spreader that had a diagonal design where the width increased as the cross-shaped heat spreader reached the edge of the "cube". This design allowed more cross-sectional area for conduction and more surface area for convection (see Fig.9) However, due to manufacturing considerations, a second mesh design was made where the lateral dimensions of the cross-shaped heat spreader were completely orthogonal (see Fig. 10).

For the air channels of the first two meshes, the air was modeled as "stagnant air", causing the air channels to act as a thermal insulator. In another variation, a third mesh was created where the heat spreader was again orthogonally shaped, but the air channels were now modeled by specifying an average convection coefficient for the natural air convection inside the channels.

For the three above meshes, regardless of how the air channels were modeled, the heat spreader placed in contact with the outer surface of the "cube". In a fourth mesh, the heat spreader configuration was modified so that the heat spreader was extended parallel to the outer surface of the "cube" by 3/16 inches (see Fig. 11). This configuration allows natural air convection to act upon both sides of the heat spreader.

4.2.2 Variations of Thermal Parameters

With the second, third, and fourth meshes, parametric variations in power levels, material properties, and "cube" configurations were investigated. For these meshes, the thermal effects of the air channels, the heat spreader, and the substrate material were investigated.

Three power levels and two substrate materials were investigated. The three power levels of the voltage regulator that were simulated are 3.0 W, 1.0 W, and 0.2 W. The two materials that were tested for the substrate both used polyurethane as the polymer base, but two different fillers were tried. The first composite consisted of polyurethane and 15% aluminum (by mass). The second composite consisted of polyurethane and 17% nylon (by mass). The conductivity of the first composite was found to be approximately 0.7 W/m K and is about double that of the nylon-polyurethane composite.

Different configurations for the "cube" were also investigated. Three configurations were made from each of the mesh variations discussed above. The first configuration consists of the "cube" with a heat spreader and air channels, the second has just a heat spreader, and the third has neither a heat spreader nor air channels.

4.2.3 Thermal Analysis of Numerical Simulations

To discuss the effects of the various parameters on the heat transfer of embedded electronics, three tables showing the results of numerical simulations were constructed. For each result shown, the ambient temperature is 25.0 °C.

Table 9 presents the effect of the geometry of the heat spreader and of the convection coefficient on the maximum temperature. Comparison of case B with case C shows that air flow through the air channels is important. When the air is completely still (no natural convection), the air acts as a thermal insulator. However, modeling the air with natural air convection, as in case C, the air channels act to enlarge the exposed surface area by which convective heat transfer can take place. Thus, maximum temperature of case C is 4.0 °C less than that of case B.

Case A and case B, in Table 9, show the result of increasing the exposed surface area of the heat spreader. In case A, the heat spreader exposed to the outside air has 250% more area than the heat spreader of case B, however, the decrease in the maximum temperature is not that significant (a change of only 11% above the ambient temperature). This shows that for this particular power level (3.0 W), the surface area of case B is sufficient for heat removal. For higher power levels, the additional surface area would be more critical in order to reduce the maximum temperature.

In Table 10, the effect of the material choice of the substrate as well as the effect of the power level is shown. As the power level increases from 0.2 W to 1.0 W, the change in the temperature rise from ambient to the maximum temperature (the temperature rise of the voltage regulator) also changes, but instead of changing by a factor of 5, the temperature rise changes by a factor of 4.15. Likewise, the three-fold increase in power from 1.0 W to 3.0 W is accompanied by only a 290% increase in the temperature rise. Therefore, the change in the power level is not directly proportional to the change in the temperature rise of the voltage regulator when the heat spreader is in contact with the surface of the substrate.

To account for this lack of linear proportionality in the relationship between the temperature rise and a change in the power level, the following formulation is useful.

$$\Delta T = R_{th} \cdot P \quad (1)$$

where ΔT = the temperature change ($^{\circ}\text{C}$)
 R_{th} = the overall thermal resistance ($^{\circ}\text{C}/\text{W}$)
 P = the power level (W)

The overall thermal resistance is a combination of the thermal resistances due to conduction and convection, R_{cond} and R_{conv} » respectively. Thus:

$$R_{th} = R_{cond} + R_{conv} \quad (2)$$

The equations giving the conductive and convective thermal resistances are:

$$R_{cond} = \frac{L}{k \cdot A_{cr}} \quad (3)$$

$$R_{conv} = \frac{1}{h \cdot A_{surf}} \quad (4)$$

where L = the material thickness (m)
 k = the conductivity of the material (W/m K)
 A_{cr} = the cross-sectional area perpendicular to the heat flux (m^2)
 h = the heat transfer convection coefficient ($\text{W}/\text{m}^2 \text{ K}$)
 A_{surf} = the exposed surface area for convective heat transfer (m^2)

Because the conductive resistance depends only on the geometry and material of the "cube", the conductive resistance is independent of the power level used (assuming the conductivity of the material to be constant and not change significantly with temperature). Likewise, although the convective resistance term is highly dependent on air flow conditions that determine the value of the convection coefficient, the convection coefficient is fixed in the simulations and does not depend on the temperature (which would affect the convection due to buoyancy effects). Therefore, for each mesh design, the temperature rise should change linearly with the power level in the numerical simulations.

A thermal resistance network as shown in Figure 12 may shed some light on the thermal situation. This resistance network is only an approximation of the physical situation but shows that the thermal resistances take the form of the "wheatstone bridge", the electrical engineering equivalent. This is the reason for the non-linear results.

If, however, the "cube" consists of the polyurethane substrate only, the thermal resistances would be expected to stay constant as power changes. This is, in fact, observed in the numerical simulations. For the nylon-polyurethane "cubes" without heat spreaders or air channels, the ratio of AT to AP is practically the same.

Table 11 shows the effect of the air flow through the air channels. Case C has the highest temperature since it has no heat spreaders or air channels. Cases B and D have no air channels either but do have heat spreaders. The fact that case B has a slightly lower temperature (even though its heat spreader is not extended from the surface) is a consequence of the modeling of the voltage regulator which is different in the two cases. The modeling of the voltage regulator in case B is slightly more accurate in that more layers were used. The temperature of case E is lower than that of case A because of the natural convection in the air channels of case E. Finally, the air channels in case A act as an insulator (since air is modeled as completely stagnant) causing case A to have a slightly higher temperature than case B. From this, it can be summarized that the air channels may help add surface area to the heat spreader for heat dissipation, but the heat spreader, itself, remains more critical than air channels alone for heat removal.

3.4 Thermal Resistance Model of the "Cube"

To analyze the relative contributions of the heat spreader and the substrate in the removal of heat from the embedded voltage regulator, a thermal resistance model is constructed to approximate the heat flow paths. Because the mesh design with the surface heat spreader produces a nonlinear relationship between AT and AP, the thermal resistance model is based upon the extended heat spreader design. The thermal resistance network is simplified to that of Figure 13.

Equations (2) and (4) provide the formulations for the the conductive and convective resistances. Table 12 shows the values that were used in the model. Determining the appropriate lengths and cross-sectional areas of the conductive resistances is difficult, and only approximations can be made. However, the exact values of the conductive and convective resistances are not needed to understand the thermal behavior of the "cube".

The values of the conductive resistance from the voltage regulator to the surface of the substrate and from the heat spreader to the surface of the substrate are approximately the same. Because of the high conductivity of aluminum, the conductive resistance of the heat spreader from its center to its outside surface is less than the other conductive resistances but still in the same order of magnitude. However, the convective resistances of the substrate and heat spreader were larger than their corresponding conductive resistances. In fact, the convective resistance of the heat spreader is almost 10 times larger than its conductive resistance. Therefore, in the design of embedded wearable computers where the surface convection coefficient cannot be controlled and the volumetric size is minimized, two parameters become critical in the thermal design: the conductivity of the substrate and the exposed surface area of the heat spreader. These two parameters, if successfully optimized, can make the wearable computer much more thermally reliable.

To ascertain the accuracy of the thermal resistance model, it is compared with numerical simulations of a "cube" having the same geometry and material properties. Results show that the predicted temperature rises of the thermal resistance model are approximately 25% less than those of the numerical simulations. This error, though significant, does not strongly affect the capability of the model to predict the heat flow paths. For the 3.0 W case, the data from the numerical simulations indicate that approximately 30% of the heat is dissipated from the heat spreader by natural convection; the model predicts 29%. However, this fractional value of heat being dissipated by the heat spreader does not fully account for the importance of the heat spreader. By spreading the heat laterally within the substrate, the heat spreader lessens the effective conductive resistance of the substrate (ie. $R_{s,cond}$ is reduced to $R_{e,q}$ by the heat spreader).

4.3 Embedded Electronics Experimentation

Physical experimentation is needed as a verification of the numerical simulation and as a test of the manufacturability of the proposed design. In some instances, physical experimentation is necessary to obtain critical information before a numerical simulation can be done, such as determining the thermal conductivity of a material.

4.3.1 Manufacturing Process

An embedded electronics "cube" consists of the following parts: the mold, the polymer composite, the heat spreader, the electronics, and the thermocouples. Described below is the general process that was taken to manufacture the polyurethane-nylon "cube", shown in Fig. 14, with the heat spreader, air channels, and the embedded voltage regulator.

To form the outer shape of the experimental artifact, a mold is made consisting of aluminum plates taped together to form the lateral, rectangular shape needed for the polyurethane composite. The heat spreader, however, introduces a complication because the design calls for the air channels to extend from the outer surface of the "cube". In order to need only one rectangular mold, the arms of the heat spreader are bent vertically upwards and later are bent away from the surface. The preparation of the polyurethane-nylon composite simply consists of mixing two-thirds polyurethane with one-third nylon powder by volume. The blend is then poured into the mold to a depth of 1.0 inches. When completely cured, the air channels are cut with a milling machine.

The aluminum heat spreader is fixed onto the top of the air channels using a thermal adhesive. The heat sink of the voltage regulator is fixed to the center of the heat spreader using the thermal adhesive. Exactly 1.0 W of heat is generated by the voltage regulators using a custom-made board consisting of diodes, capacitors, and carbon resistors. This board is connected to the voltage regulator by wires and therefore can be used by other "cubes". After the thermal adhesive dries, the polyurethane-nylon composite is poured to a height of 1.0 inches above the top of the voltage regulator. After the composite cures, the holes for the thermocouples are drilled with good precision (± 0.02 inches), and the locations of the thermocouples are recorded. The gap between the thermocouple and drilled hole is filled with the polyurethane-nylon composite. The locations of the thermocouples correspond to locations used in the numerical simulations for comparison purposes.

4.3.2 Embedded Electronics Experimental Procedure

A DC voltage source supplies the embedded voltage regulator with power. Before the power is turned on, the thermocouples are connected to an analog-to-digital (A/D)

board which is operated on an IBM 386 computer using software specifically written for the purpose of data acquisition for the thermocouple temperatures. The user inputs the number of thermocouples, the ambient temperature, the length of time the experiment will be run, and the time between readings.

The calibration of the A/D board is done by placing two thermocouples of the same variety in a boiling beaker of water. One thermocouple is connected to a handhold pyrometer, and temperature measurements are written down every 30 seconds. The other thermocouple is connected to the A/D board, and its values are also read every 30 seconds. A simple algebraic formula is then made to adjust the A/D boards values with that of the handhold pyrometer. This is then encoded in the software.

4.3.3 Experiments Performed on Each "Cube"

Once the cube is manufactured, six experiments are performed by varying the air flow conditions within the air channels and over the outer surface and by varying the power level produced by the voltage regulator. One experiment simply consists of taping the end of the air channel, thus creating the condition of stagnant air inside the air channels with natural convection operating on the extended heat spreader. In the last experiment a small fan (with a known air flow rate) will be used to move air across the entire "cube". For each of these experiments, two power levels shall be tested: 1.0 W and 3.0 W.

4.3.4 Types of Manufactured Polyurethane Composite "Cube"

Several types of "cubes" will be manufactured so as to test the various parameters of interest, namely the heat spreaders and choice of filler for the polyurethane-filler composite. The first "cube" manufactured has air channels and an aluminum heat spreader and consists of a polyurethane-nylon substrate having 17% nylon by mass. This "cube" has shown that the manufacturing technique is satisfactory and that physical experimentation is feasible in verifying the thermal predictions of the numerical simulations.

Two additional "cubes" are also to be manufactured. The first investigates the effect of a layer of a high conductivity filler used with the polyurethane (for example,

copper). This layer is placed at the level of the heat-producing components and would take the place of the heat sink. A thin layer of the composite with copper coats the outside of the surface, acting as an enlarged heat spreader. The majority of the substrate uses aluminum oxide as the filler. The second "cube" to be manufactured will have an aluminum heat spreader and air channels but will be made of a new resin with aluminum oxide particles comprising 70% of the composite by volume. The new resin is a bisphenol F epoxy and with the aluminum oxide filler is reported to have a conductivity as high as 4.5 W/m K, a six fold increase from the conductivity of the polyurethane-aluminum composite (15% aluminum by mass) used previously.

4.4 Determination of the Conductivity of a Composite Material

When modeling the heat transfer aspects of any object, the most important property to know is its conductivity. Because not all materials used in physical experiments are given a specified thermal conductivity, several ways have been developed to approximate the conductivity. Although the determined value of the conductivity is only approximate, the information is much needed in order to proceed with the numerical simulations.

4.4.1 Analytical Methods

A very rough estimation of the conductivity of a composite material can be made by analytical formulations. If the percent composition of the constituent components is known as well as their respective conductivities, a thermal resistance approach can be used. Two analytical formulations have been developed to estimate the maximum and minimum effective conductivities possible for the conductivity. The upper and lower limits of the conductivity of the composite depend on the configuration of the materials with respect to the direction of the heat flow. Modeling the heat transfer as either a series or parallel thermal resistance network helps to analyze the possible configurations.

The series thermal resistance network places a lower bound on the conductivity. Since the heat must flow through both materials, the less conductive material has its largest possible effect on the overall conductivity in this configuration, causing the lower limit of the conductivity of the composite to be ascertained. The series formulation takes the form of:

$$k_{\text{composite}} = \frac{k_a k_b}{v_a k_a + v_b k_b} \quad (5)$$

where v is the volume fraction of the constituent materials and k the conductivity. The volume fraction is used as a basis for measuring the relative thickness of the each layer of the individual materials.

The parallel resistance network, on the other hand, produces the upper limit of the conductivity of the composite because the heat is allowed to mostly bypass the less conductive material and flow through the higher conductive material. Its formulation takes the form:

$$k_{\text{composite}} = v_a k_a + v_b k_b \quad (6)$$

It must be noted, however, that more accurate formulations have been developed to determine the conductivity of a polymer-filler blend such as the ones being used in our experiments.(Bigg, 1986).

4.4.2 Line Source Method

One method for determining the conductivity of a composite material is to compare numerical simulations with experimental results. This is an unsteady-state technique that does not require the materials to reach their steady-state temperature (Bigg, 1986). This procedure determines the approximate conductivity of the polyurethane-aluminum oxide composite that is 15% aluminum by mass.

The polyurethane-aluminum oxide composite was poured into cylindrical mold with a carbon resistor inside. After the composite cures, four thermocouples are embedded inside (see Fig. 15) at predetermined locations corresponding to locations prescribed in the numerical simulations. Several experiments were run to obtain the thermocouple temperature results corresponding to a particular power level.

A mesh for the numerical simulations is constructed for the prescribed geometry and thermocouple positions. Many numerical simulations are run with each using a slightly different conductivity to compare its temperature predictions with those observed

in the experiment. From this approach, a conductivity of 0.7 W/m K is ascertained for the polyurethane-aluminum oxide composite with a reasonable uncertainty of +/- 0.1 W/m K.

4.4.3 Heat Flux Experimental Method

A more direct method for obtaining the conductivity of a composite material employs a heat flux sensor and heat flux generator to model a one dimensional heat transfer problem for which the conductivity is readily determined (see Fig. 16). This is a steady-state technique requiring two to 24 hours to complete (Bigg, 1986).

A 0.5 inch diameter microfoil heat flux sensor made by RdF Corporation is sandwiched between a 0.5 inch diameter thermofoil heater made by Minco Products, Inc. and a 0.5 inch diameter specimen of unknown conductivity with a thickness of 0.0625 inches. The thin profile of the specimen will insure the validity of the one dimensional model. Knowing the heat flux going through the face of the specimen and the temperature on each side of it using thermocouples, the conductivity of the specimen will be determined more accurately than the "line source method" described above.

4.5 Factors Affecting the Conductivity of a Polymer-Filler Composite

Polymers may be made more conductive by adding conductive fillers to the polymer matrix. The conductive fillers are very fine particles on the size of hundreds of μm and typically have a conductivity of at least 20 W/m K. The parameters that can be varied in the selection of the filler are its conductivity, particle size, aspect ratio, orientation, and volume fraction.

As long as the conductivity of the filler is two orders of magnitude higher than that of the polymer, the conductivity of the filler has very little effect on the conductivity of the composite (Bigg, 1986). The particle size has little effect on the conductivity of the composite as well. However, as the particle size increases, the resulting heterogeneous character of the composite makes it more difficult to predict its conductivity. The greatest effect on the conductivity of the composite is produced by the volumetric packing fraction of the filler. As the volume percentage of the filler increases, the conductivity of the composite increases exponentially.

Typical filler materials that are used to enhance the conductivity of the composite are copper, silver, aluminum, tin, aluminum oxide, silicone, and carbon. (Bigg, 1986). Two filler materials that have very promising results are aluminum nitride (Bujard and Ansermet, 1989) and boron nitride (Bujard, 1988). Conductivities for composites with these materials can approach 4 w/mk and 5 W/m K, respectively.

For fibers that have large aspect ratios (long and thin particles), the orientation can have a significant effect since a conductive path can be created from the chain of the filler particles. Chains structures of the filler particles increase with increasing volume fractions making it more difficult to predict the conductivity of the composite as the volume fraction is increased.

A model has been developed to predict the conductivity of polymer-filler composites that agrees well with experimental results. The model was developed by Nielsen and is a generalization of the Kerner calculation used for determination of the hear modulus of solids (Bujard, 1986). Nielsen's model assumes the particles to be randomly scattered and have no thermal resistance of the interface between the particles and the epoxy. The following is Nielsen's model:

$$\frac{k_c}{k_p} = \frac{(1 + ABO)}{(1 - B\phi\Phi)} \quad (7)$$

where k_c = the conductivity of the composite
 k_p = the conductivity of the polymer
 k_f = the conductivity of the filler

$$A = \frac{k_f}{k_p - 1} + \frac{k_f}{k_p}$$

$$\phi = 1 + \frac{1 - O_m}{\Phi m^2} \Phi$$

A = factor depending on particle geometry
O = volumetric ratio of filler
 O_m = maximum volumetric packing fraction for the filler

5. Conclusions

Applying heat transfer principles to wearable computers requires that the thermal design develop concurrently with the designs of the electronic and industrial design teams. Without concurrent design, the thermal concerns cannot be adequately addressed in the short design cycle, causing the thermal design to become little more than an afterthought. Concurrent thermal design should develop in three basic stages. First, the basic type of cooling arrangement is chosen. Second, the actual devices needed for the cooling arrangement are selected and their implementation tested. Lastly, a numerical model is constructed to assess the effectiveness of the overall thermal design.

The Navigator 2 is a design based on the framework of concurrent engineering. In its development, heat spreaders were found to be the simplest and most satisfactory way of transporting the heat from the electronic components. Thus, the thermal design concentrated on the most efficient medium to convey the heat to the heat spreader, through the heat spreader, and from the heat spreader into the ambient air. The design calls for a thermal interface material to minimize air gaps between the components and the heat spreader as well as a large outer surface area to minimize convective resistance to the ambient air.

Embedded electronics is a novel approach to the thermal problems of portable, wearable computers. Because air is generally an insulating medium when stagnant and forced-air cooling requires both increased space and power, conduction is seen as a way of transporting heat from the electronics to the environment. To maximize the conduction of heat, a combination of heat spreaders and polymer composites with conductive fillers is being studied. The heat spreader and the polymer composite work together in spreading and removing heat from the components. Their exact relationship and optimization is currently being researched.

6. References

Ahmed, L, Krane, R.J., Parsons, J., 1990, "A Preliminary Investigation of the Cooling of Electronic Components With Flat Plate Heat Sinks ," Transaction of the ASME, March 1994, Vol.116, pp.60-67.

Bigg, D.M., "Thermally Conductive Polymer Compositions," Polymer Composites, June, 1986, Vol.7, pp. 125-126.

Bujard, P., "Thermal Conductivity of Boron Nitride Filled Epoxy Resins: Temperature Dependence and Influence of Sample Preparation," Complete Manuscript Reviewed by I-THERM Program Committee, February 1, 1988.

Finger, S., Stivoric, J., Amon, C.H., Gursoz, L_M Prinz, R, Siewiorek, D., Smailagic, A., Weiss, L., 1992-1993, "Reflections on a Concurrent Design Methodology: A Case Study in Wearable Computer Design," Submitted to Computer Aided Design, Special Issue on Concurrent Design.

Johnson, R.D., "Efficient Cooling Increases Component and Equipment Reliability," April, 1987, Electrotechnology, Vol. 15, Reprinted by Technical Manager, Iree Monitor, June, 1989, Redpoint Ltd. U.K.

Lee, T., Chambers, B., Mahalingam, M., "Application of CFD Technology to Electronic Thermal Management," 1994, IEEE 0569-5503/94/0000-0411.

Mallik, A.K., Peterson, G.P. Weichold, M.H., "On the Use of Micro Heat Pipes As An Integral Part of Semiconductor Devices," Journal of Electronic Packaging, August 7, 1992.

Nigen, J.S. and Amon, C.H., 1992, "Concurrent Thermal Designs of PCB's: Balancing Accuracy With Time Constraints," IEEE Transactions on Components, Hybrids, and Manufacturing Technology, Vol.15, pp. 850-859.

Pei, H. and Larson, R., "Miniaturization of Cooling Components-An Overview," Nepcon East 93 Conference: June 14-17,1993, Bayside Exposition, Boston, Mass., Proceedings of the Technical Program, Des Plaines, IL, 1993, pp.541-8.

Rensburg, R., "New Routes to Cooler Electronics," Machine Design, July 11, 1991, pp.73-76.

Sridhar, S., Bhagath, S., and Joshi, Y., 1994, "Reviewing Today's Cooling Techniques," Computer Packaging Technology, pp. 49-55.

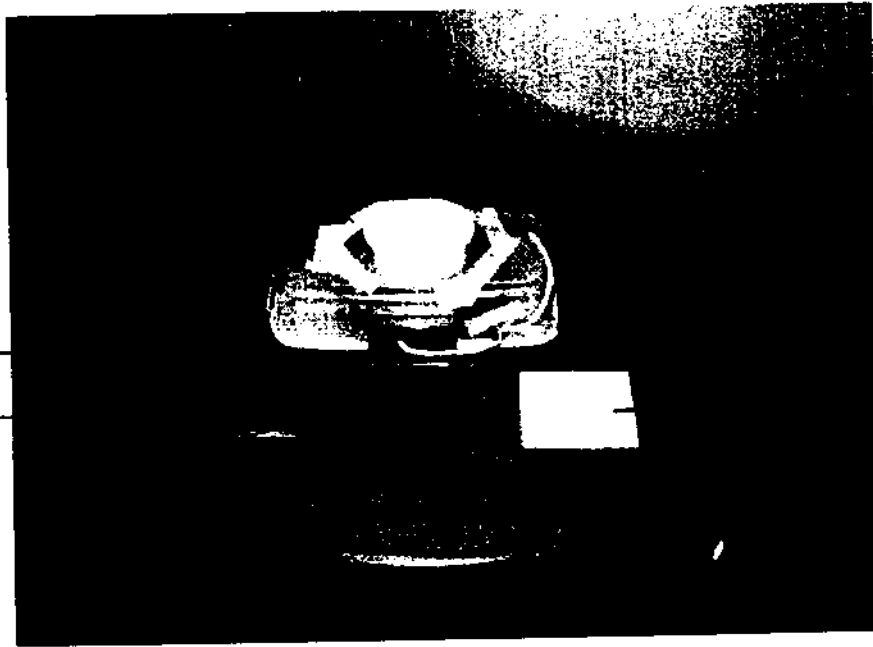
Soule, C.A..., 1992, "Water-Cooled Heat Sinks Improve Thermal Efficiency," Powerconversion & Intelligent Motion, Vol.18, pp. 18-22.

Wall, C, 1989, "Thermal Management of a Microcomputer Using a Liquid Heat Sink," Electronic Manufacturing, Vol.35, pp. 19-20.

Egan, E., 1996, Master's Project Thesis, Department of Mechanical Engineering, Carnegie Mellon University, Pittsburgh, Pennsylvania

Aluminum
Heat
Spreader

LHS



Gap Pad

Fig. 1

Voltage Regulators

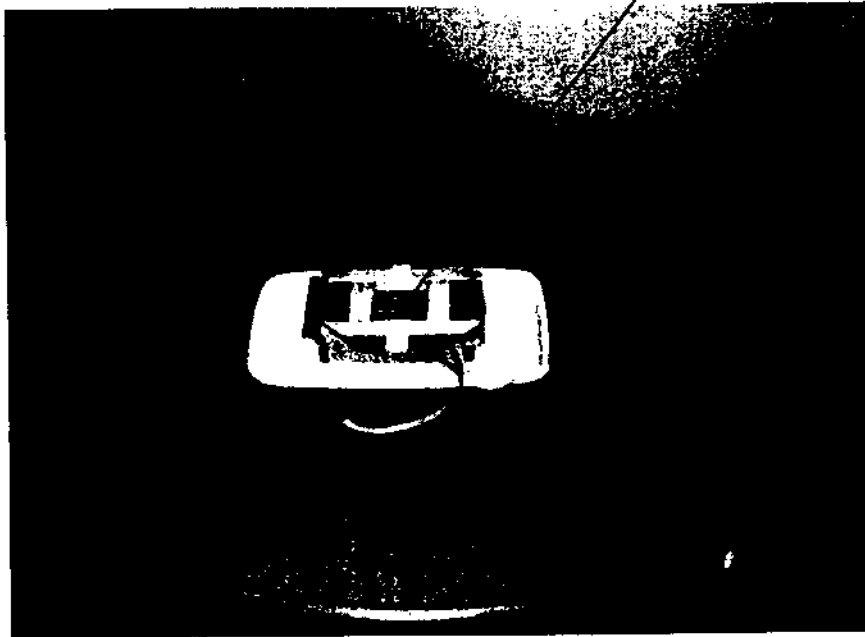
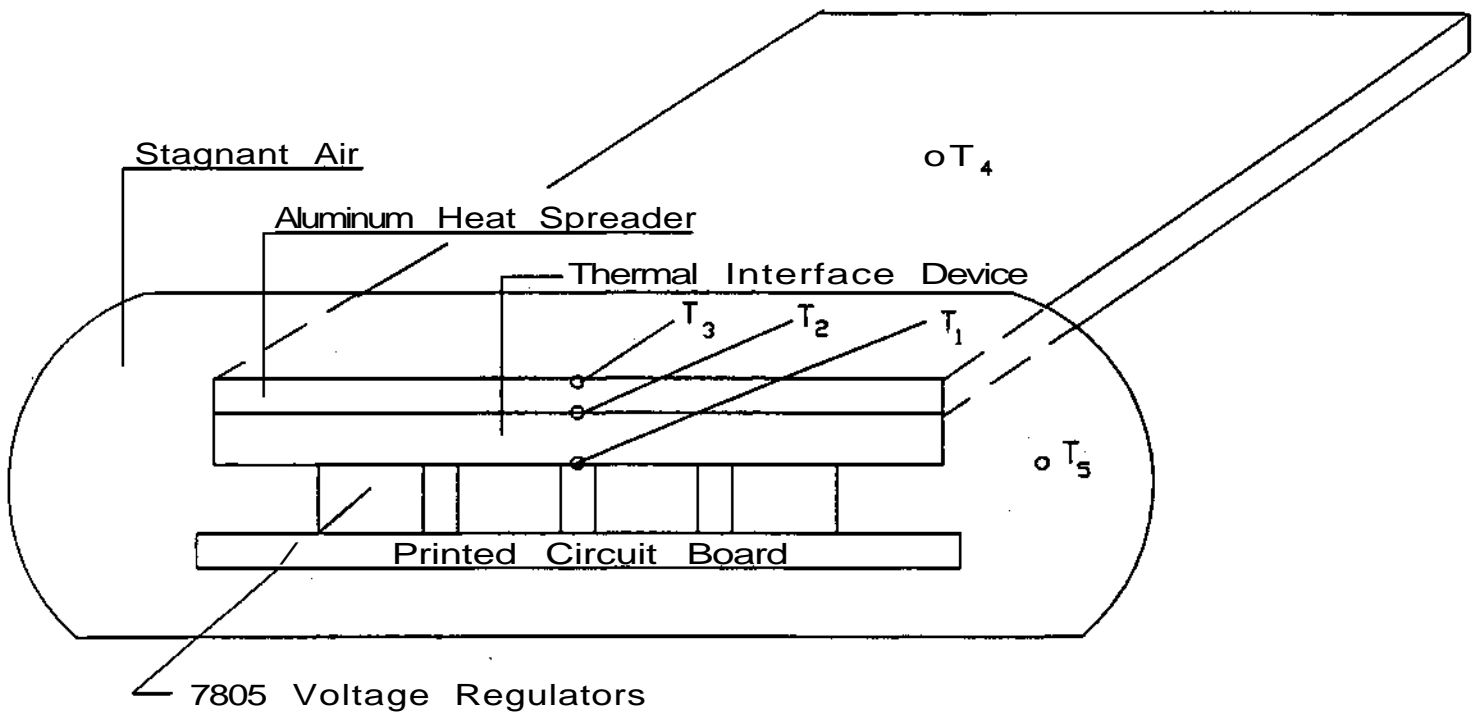


Fig. 2



Schematic of the Wearable Computer Heat Sink Test Bed

Fig. 3

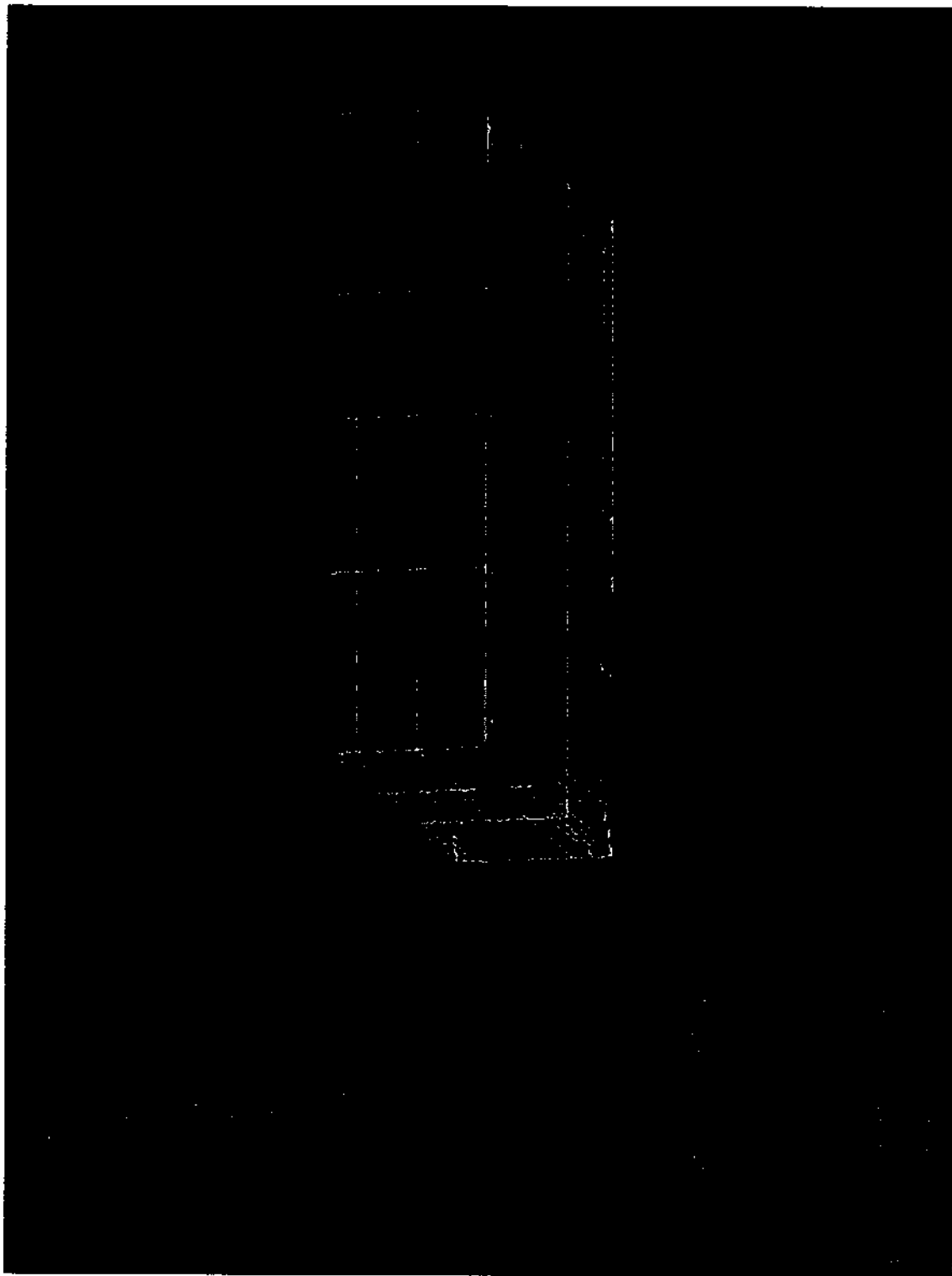
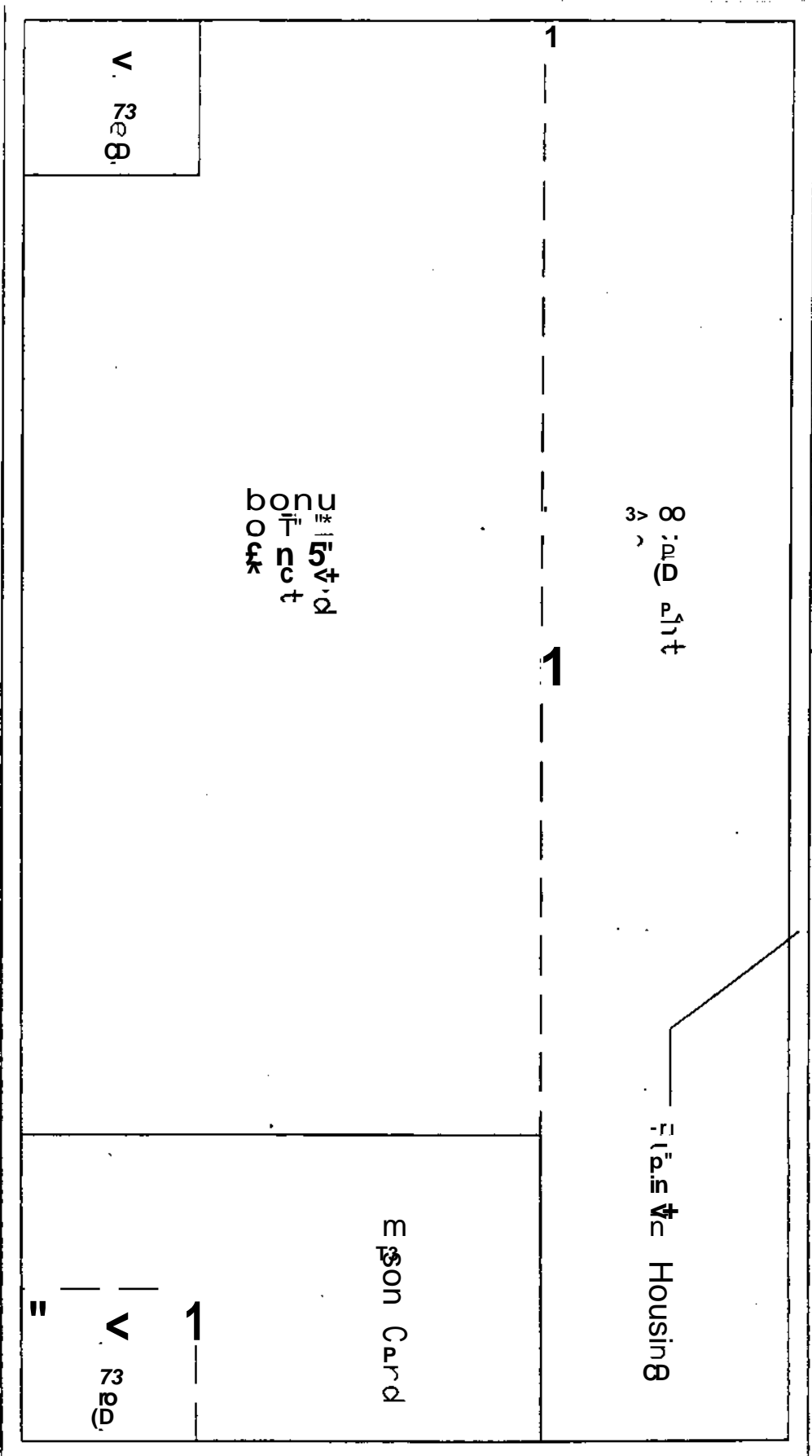


Fig. 4
Second Navier-Stokes Mesh



Horizontal View of the Navigation Mesh

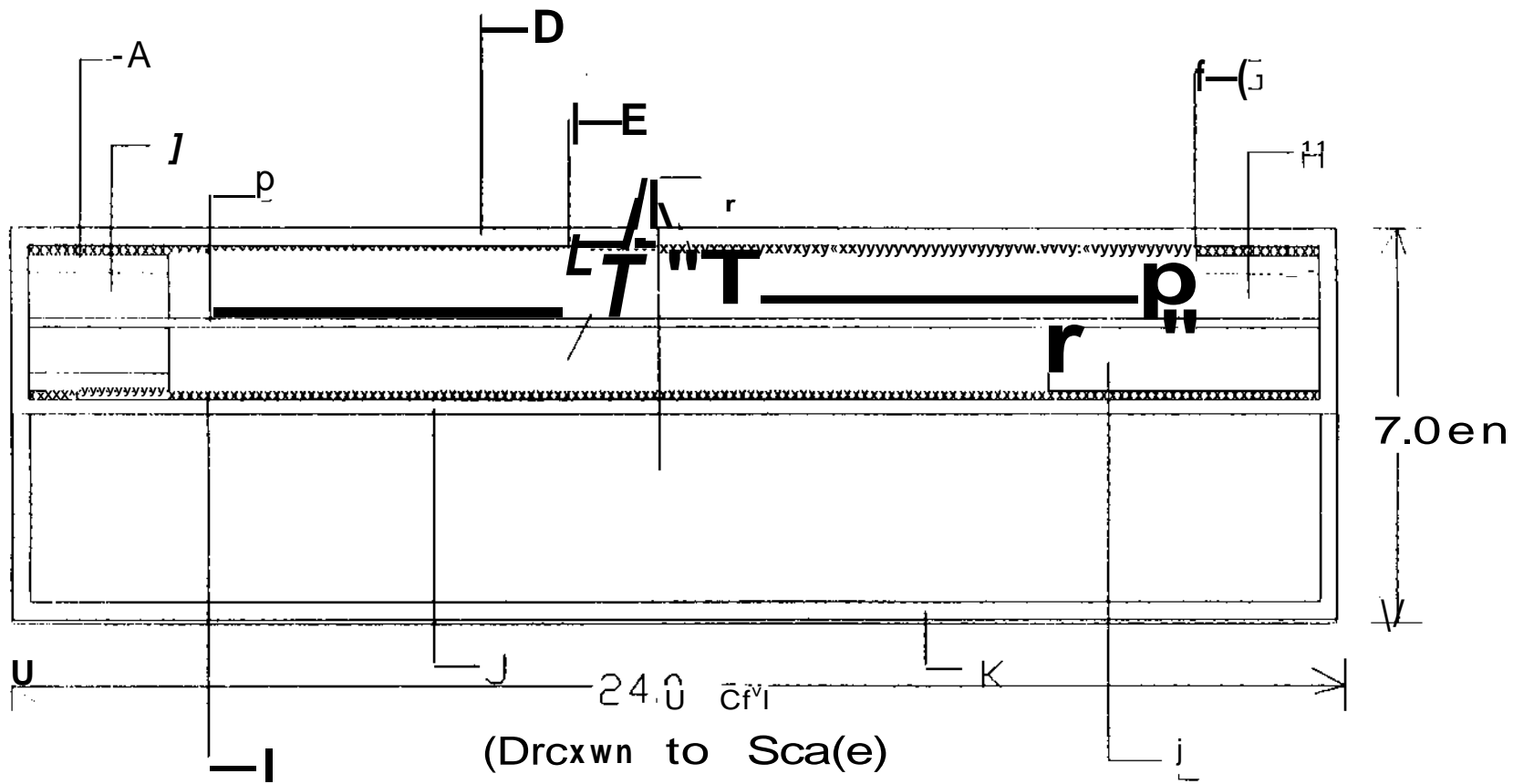
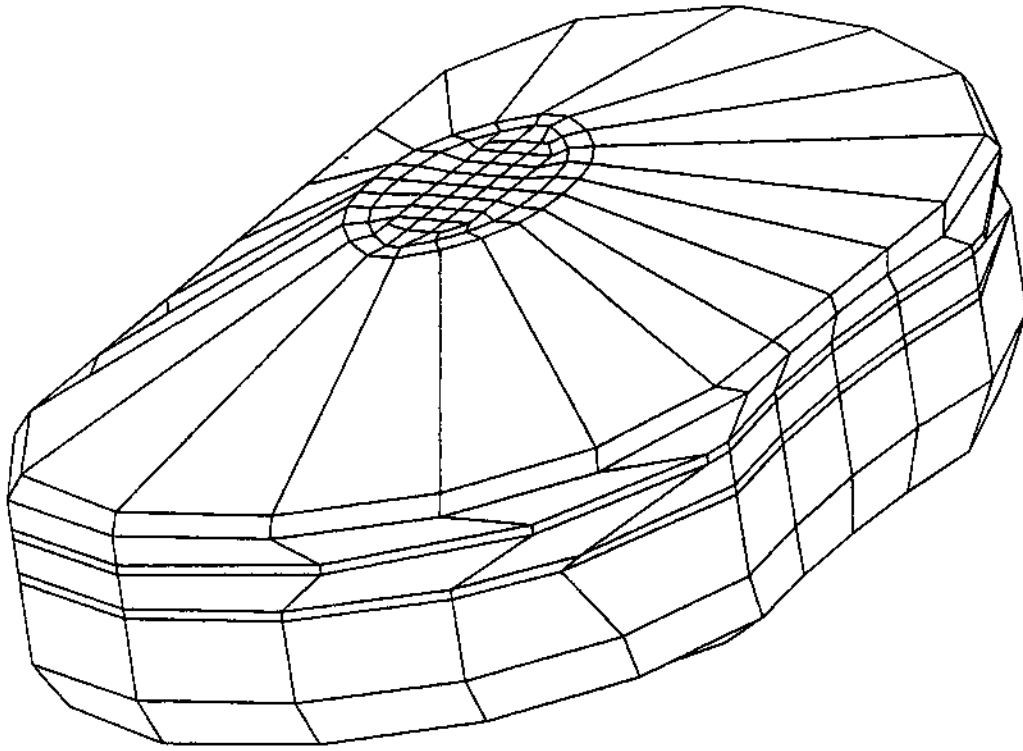


Fig. 6

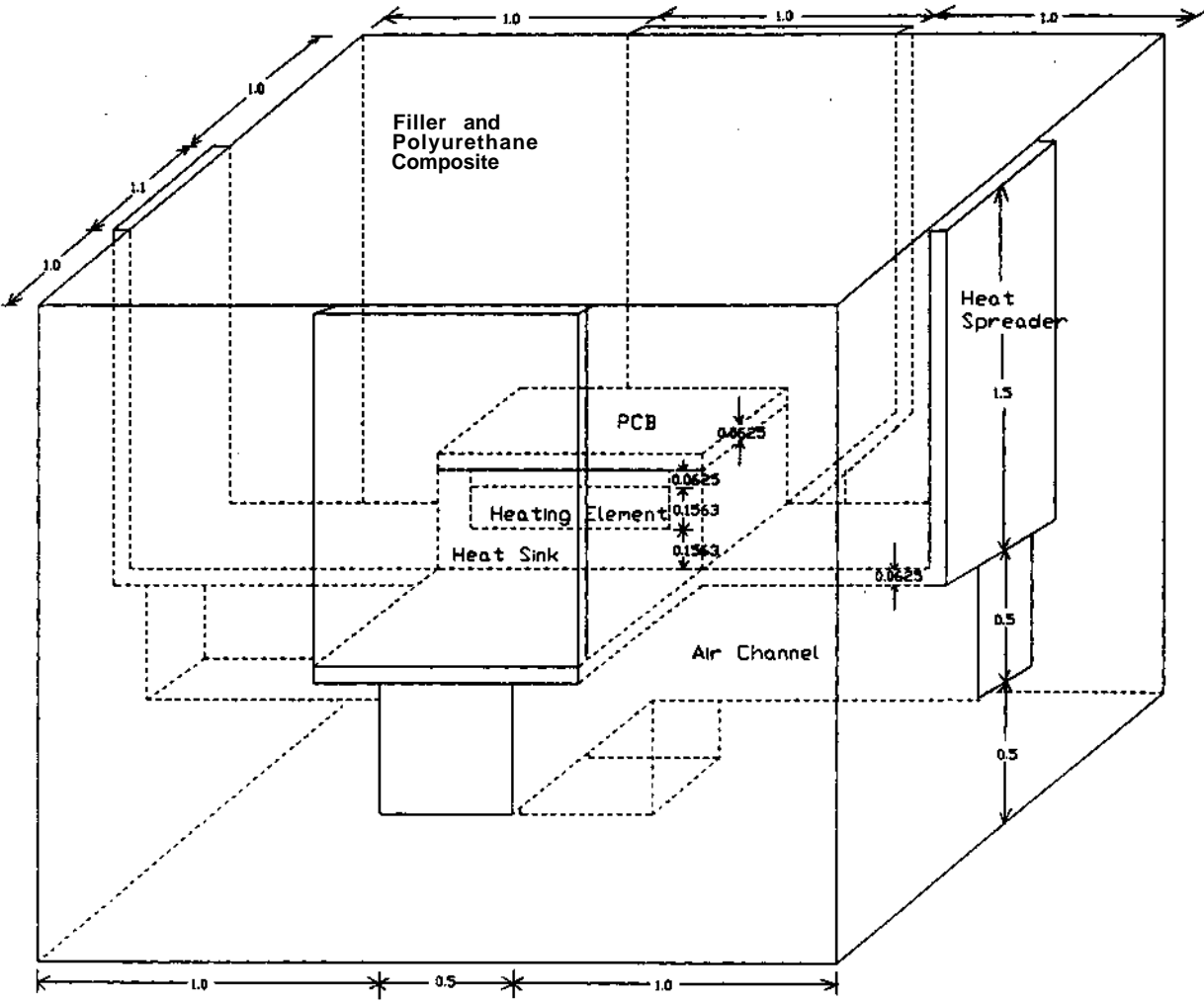
- A. Anodized aluminum heat sink
- P. 7RS130SHf; Voltage Regulator (4.5 W)
- C. 1.6V in f... Board (PCB)
- I. Gap Pad with Pressure Sensitive Adhesive
- J. Aluminum heat spreader
- E. Gap Pad with Pressure Sensitive Adhesive
- F. ... air
- G. Anodized aluminum heat sink
- H. 78SST133HC Voltage Regulator (0.75 W)
- I. Gap Pad with Pressure Sensitive Adhesive
- J. Aluminum heat spreader
- L. Epson ID-486 Cord (4.5 W)



Detailed mesh of the Navigator 2

Ft, 7

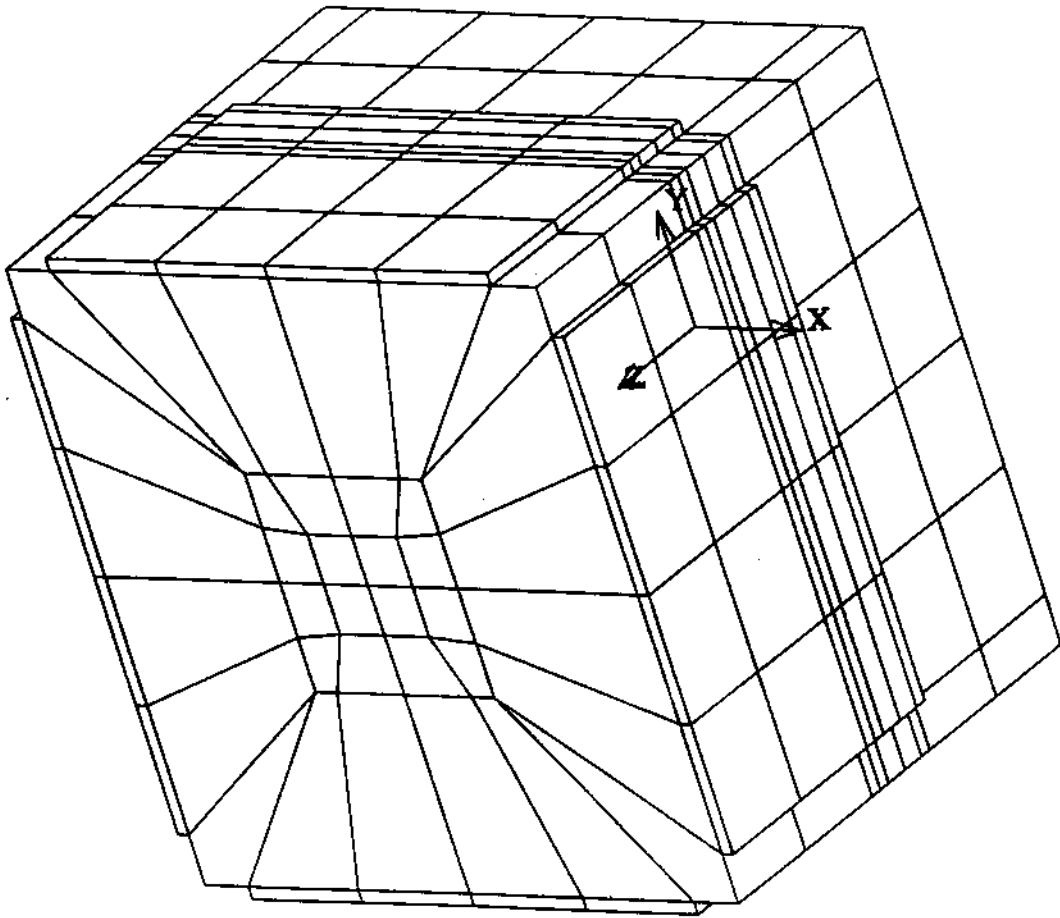
Embedded Voltage Regulator Assembly



Call dimensions in inches)

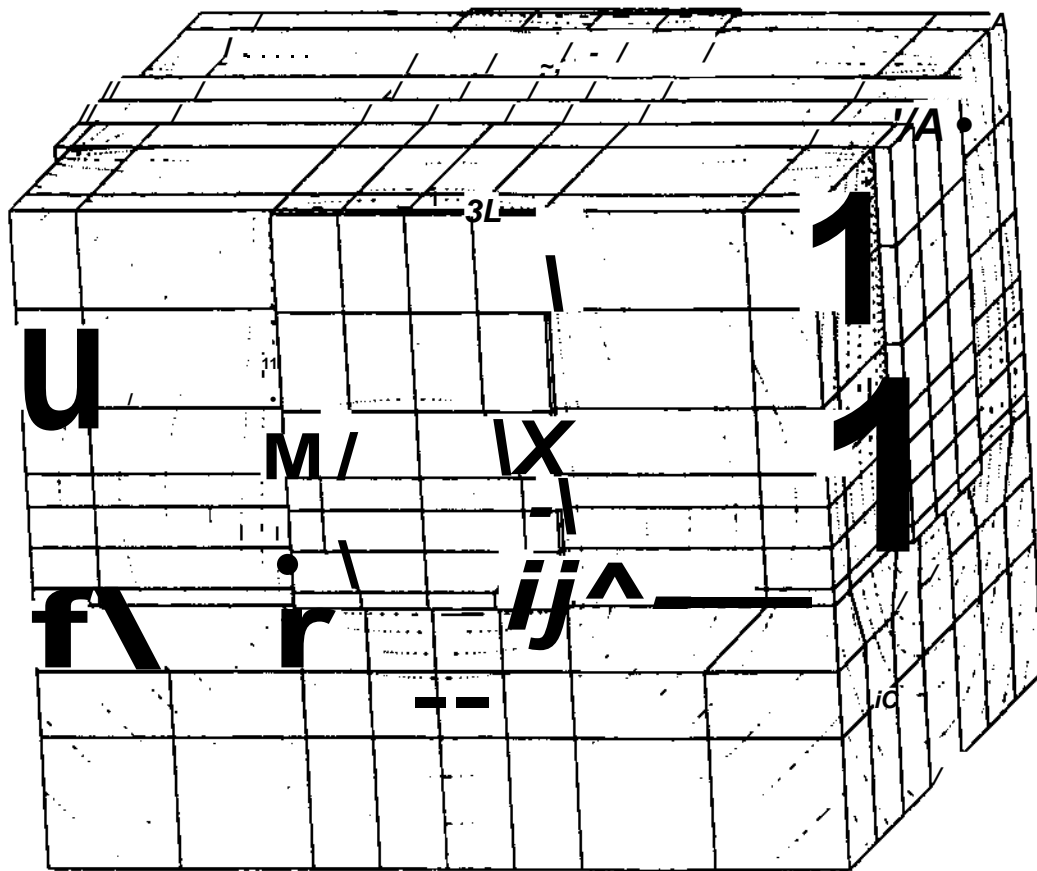
Case Study of
Embedded Electronics

Fig. 8



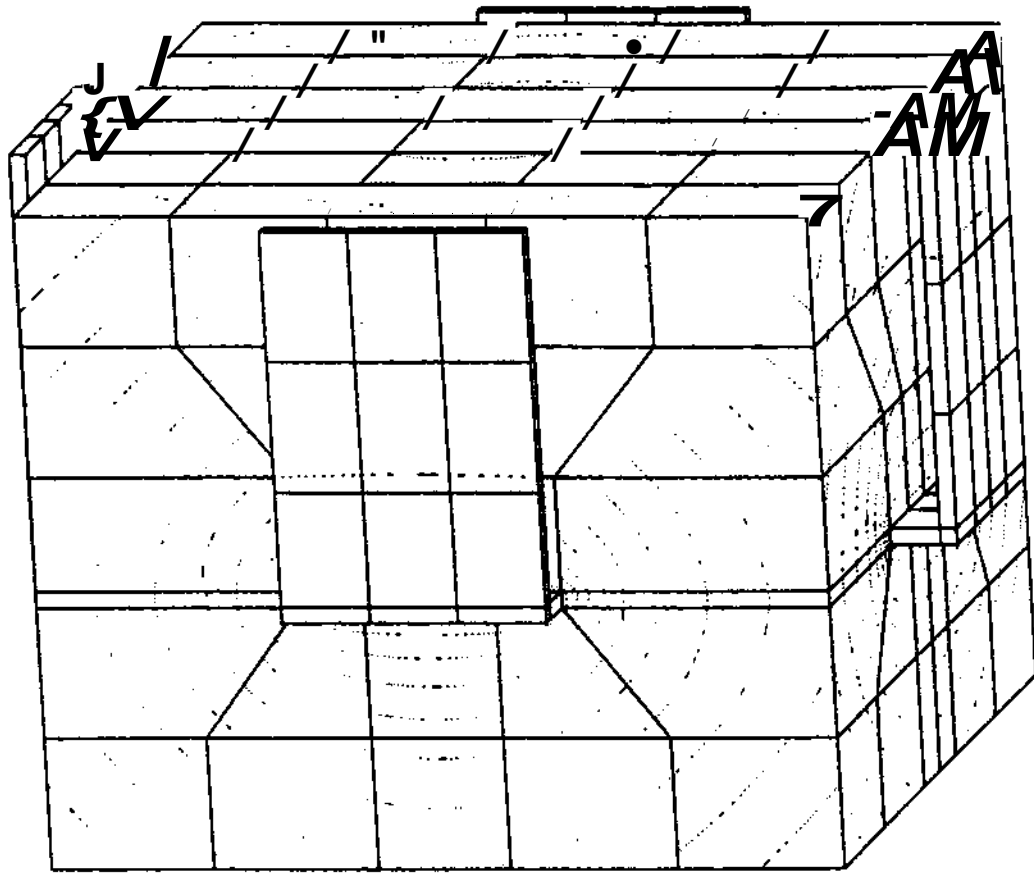
"Cube" Mesh Design with Diagonal, Surface-Contact Heat Spreaders

Fig. 9



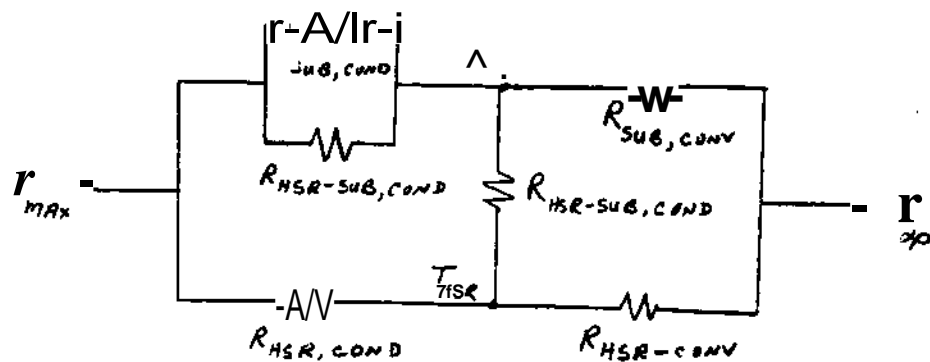
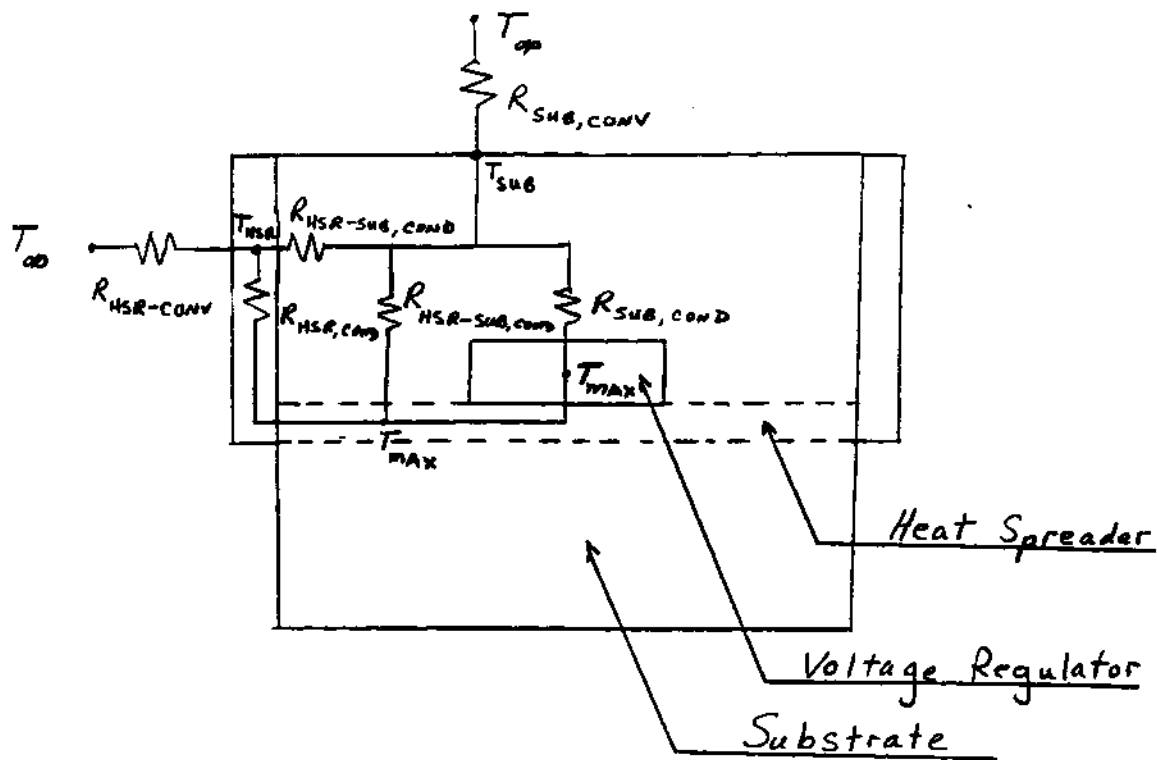
"Cotbe" Mesh Design with Surface - CoA-tact Heat Spreaders

Fig. 10



"Cube" Mesh Design with Extended Heat Spreaders

F-9% 11



Thermal Resistance Network of Heat Spreaders in Contact with the Surface

Fig. 12

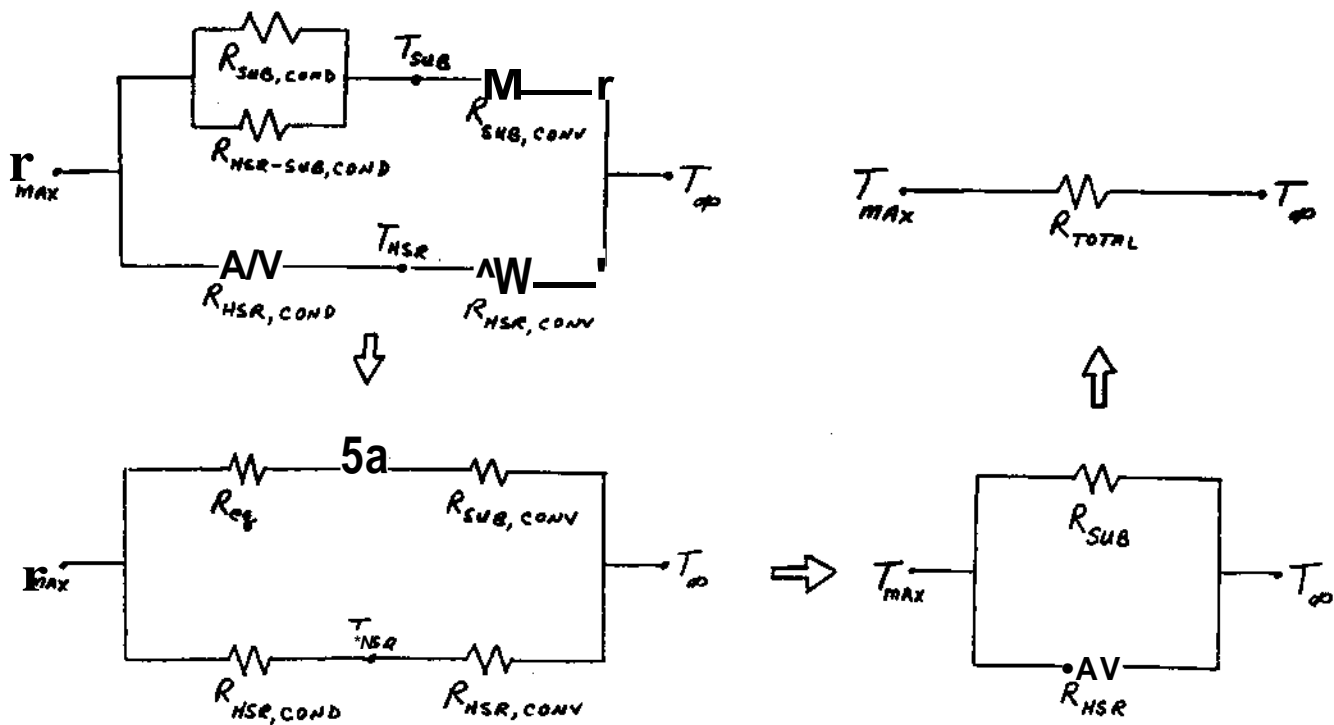
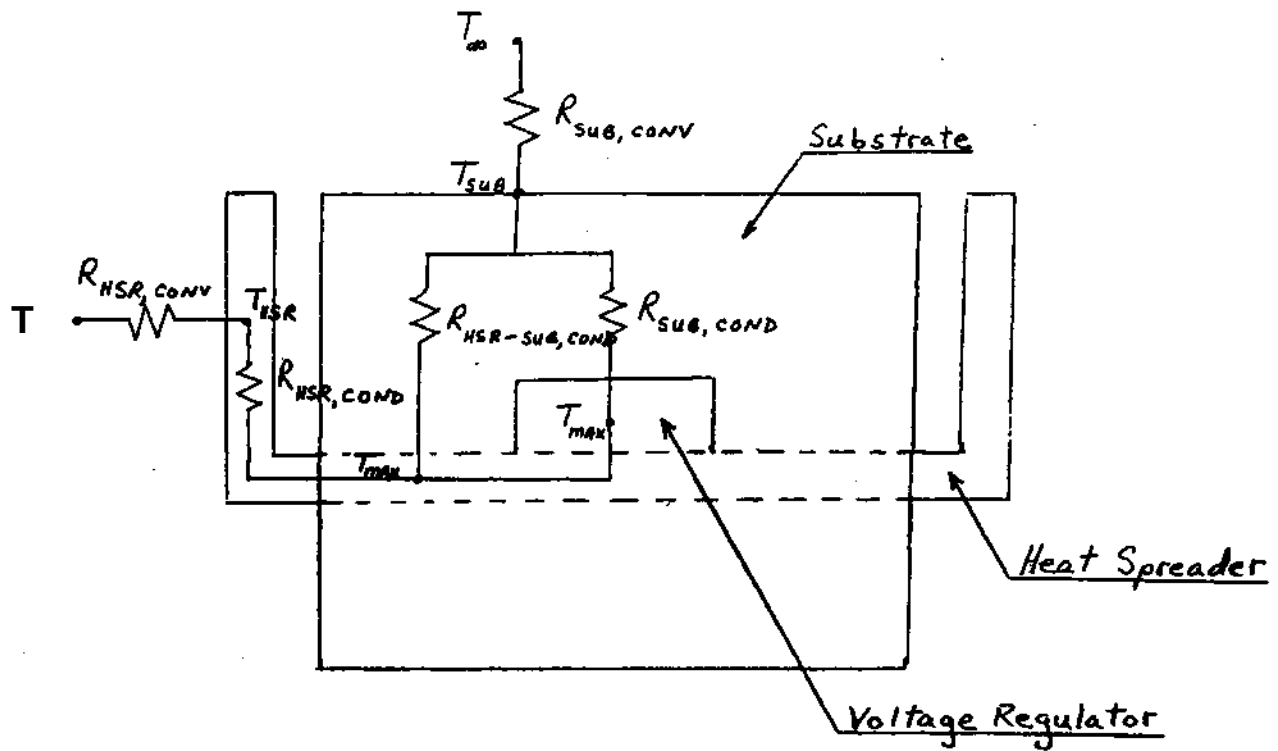


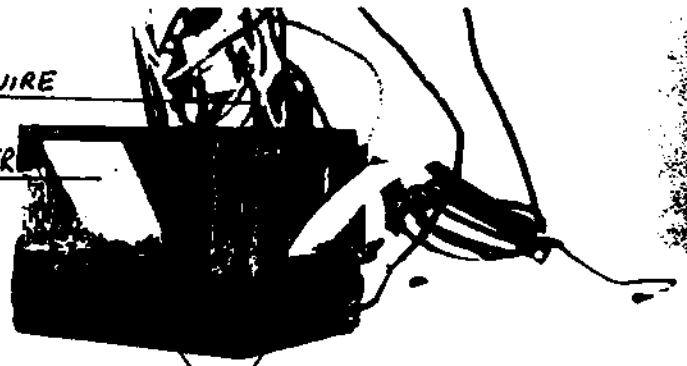
Fig. 13 Thermal Resistance Model of "Cube" w/ Extended H. Spr.'s

111010 "rapns of Nylon-Polyurethane Lube"



THERMOCOUPLE WIRE

AL HEAT SPREADER



AIR CHANNELS

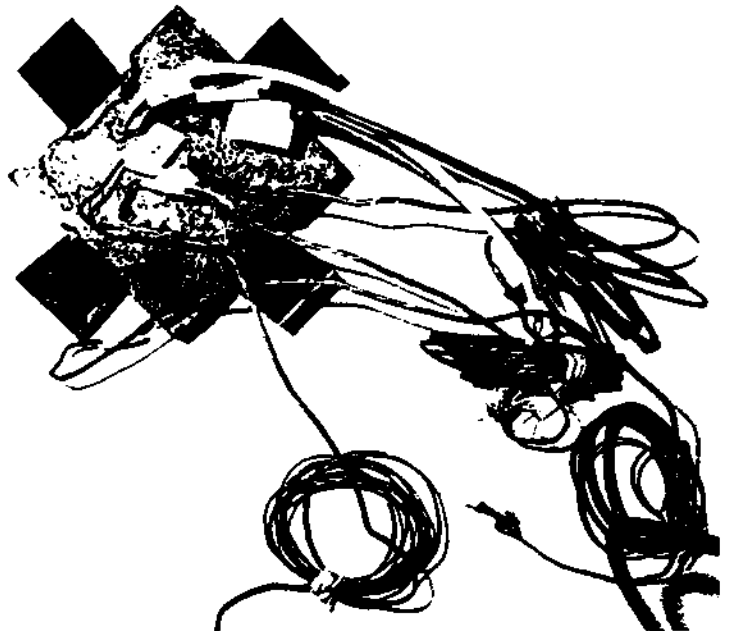
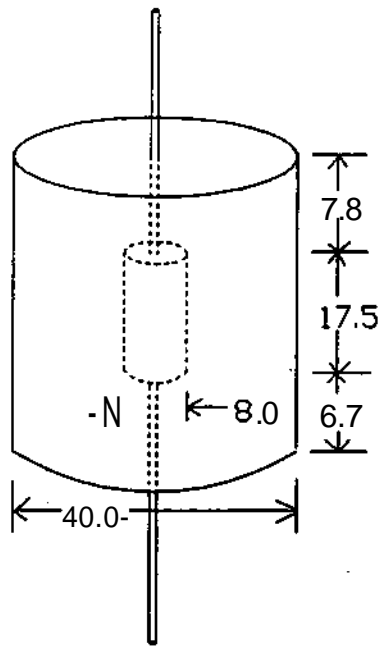
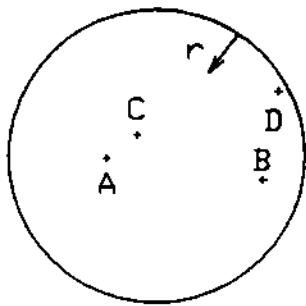
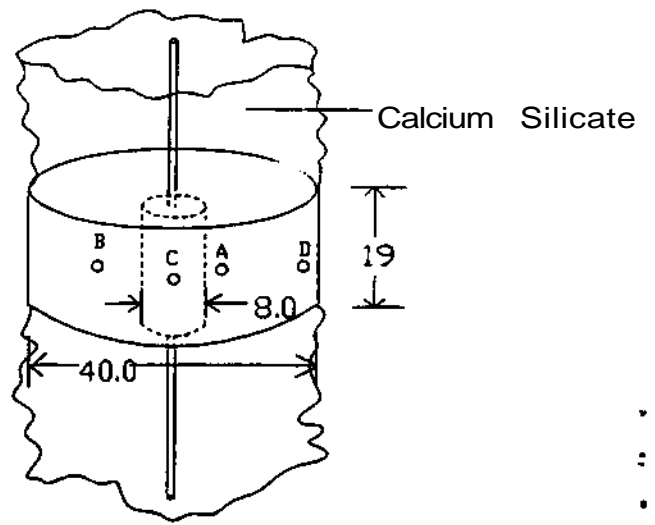


Fig. 14

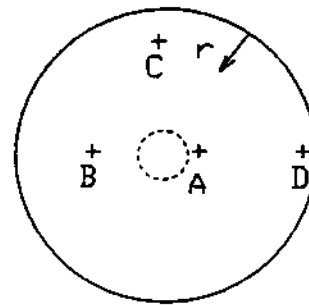
Specimen A



Specimen B
(Insulated Ends)

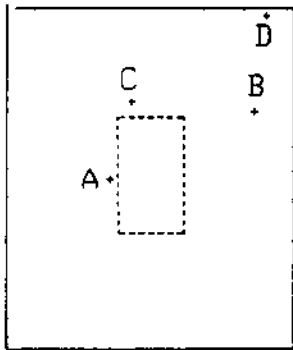


Point	h	r
A	19.6	15.5
B	8.3	9.1
C	7.5	18.7
D	5.0	2.8

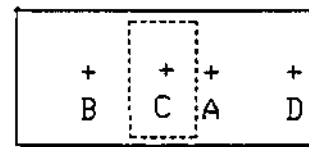


Point	h	jr
A	11	14.2
B	11	12.8
C	11	4.9
D	11	12

T



T

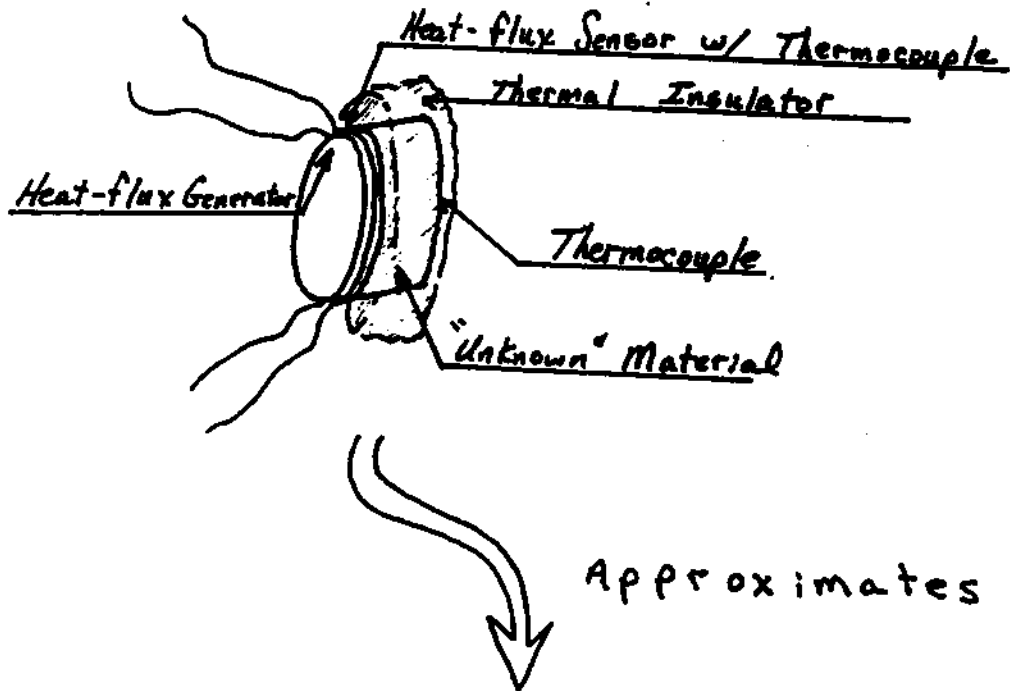


All Dimensions in millimeters

(accuracy ± 0.3 mm)

(accuracy ± 1 mm)

Alternative Property-Determination Method:



Approximates

INSULATED, ADIABATIC SIDE

$$f_a \sim \frac{J}{T} \quad T_1, T_2 \rightarrow \text{KNOWN}$$

Known

Therefore, f can be found.

Fig. 16

Table 1: Heat-Producing Electronic Components of the Navigator2

<u>Component</u>	<u>Estimated Power Operating Level (Wt)</u>	<u>Maximum Temp. (°C)</u>
Epson 10-486 Card-Type PC (with 3.3V 33 MHz 486-SL Processor)	4.5	55
78SR174HC Power Trends 7V Voltage Regulator	0.5	60
78ST305HC Power Trends 5V Voltage Regulator	1.5	60
78ST133HC Power Trends 3.3V Voltage Regulator	0.75	60
Total Operating Conditions	7.25	55

Table 2: Possible Software Power-Saving Features for the Navigator2

<u>Mode</u>	<u>Timer</u>
CPU Standby	4 seconds
Global Standby	15 seconds
Auto Suspend	5 minutes
Video	Disable
Serial 1	4 seconds
Serial 2	4 seconds
Hard Disk	1 minute
TERI Card	4 seconds

Table 3: Types of Heat Spreaders Used in Heat Sink Test Bed Experiments

<u>Designation</u>	<u>Thickness (in)</u>	<u>Area Exposed to Natural Air Convection (in²)</u>
A	1/48	36
B	1/16	36
C	1/16	108
D	1/8	108

Table 4: Temperature Data from the Heat Sink Test Bed Experiments

Exp. No.	Type of H. Spr.	Power (W)	Thermal Interface	T1	T2	T3	T4	T5	T1-5
<-----(oc)----->									
1	none	3.0	none	77.7	—	---	---	23.5	54.2
2	none	3.0	LHS	77.0	66.7	—	—	36.1	40.9
3	none	3.0	Gap Pad	80.8	75.3	—	—	35.3	45.5
4	A	3.0	LHS	66.4	50.5	46.2	33.0	26.0	40.4
5	A	3.0	Gap Pad	64.4	61.6	52.2	36.6	35.5	28.9
6	A	3.0	none	62.0	—	50.7	35.8	24.6	37.4
7	none	3.0	none	91.3	—	—	—	40.0	51.3
8	B	3.0	LHS	77.1	59.0	51.2	46.7	41.0	36.1
9	B	3.0	Gap Pad	74.6	73.7	50.1	45.3	40.5	34.1
10	B	3.0	LHS	91.2	65.5	56.4	49.5	45.1	46.1
11	B	5.0	Gap Pad	85.7	85.0	55.0	48.5	45.2	40.5

12	none	3.0	none	77.2	—	—	—	34.5	42.7
13	B	3.0	none	65.8	51.9	46.3	41.0	37.3	28.5
14	C	3.0	Gap Pad	53.6	45.2	40.5	32.0	28.9	24.7
15	C	8.0	Gap Pad	75.8	58.5	52.0	37.1	29.4	46.4
16	D	8.0	Gap Pad	70.4	57.3	46.0	38.3	27.0	43.4
17	D	8.0	*Gap Pad	66.6	60.1	50.1	40.6	27.5	39.1

* Note: Gap Pad that is 1/16 inch thick and has a pressure sensitive adhesive on the glass-fiber reinforced side.

Table 5: Comparative Temperature Rises in the Test Bed Experiments

Experiment	Thermal Interface	Ti-3(OQ)	Ti-5(°C)
4	LHS	20.2	40.4
5	Gap Pad	12.3	28.9
8	LHS	25.9	36.1
9	Gap Pad	24.5	34.1
10	LHS	34.1	46.1
11	Gap Pad	30.7	40.5

Table 6: Numerical Simulations of the Navigator2

Mesh Type	h(W/m ² K) of H.Spr.	h(W/m ² K) of sides	Exposed H.Spr. Area to Air (in ²)	k _{metal} (W/m K)	kQapPad (W/m K)	Max* Temp(°C)	
First	(a)	5	5	7	200	0.58	75.7
	(b)	5	5	7	400	1.75	75.0
	(c)	5	5	7	200	1.75	74.0
	(d)	5	5	27	200	1.75	60.6
	(e)	5	5	54	200	1.75	52.2
	(f)	5	5	81	200	0.58	48.4
Second	(g)	5	1	74	85	0.50	54.8
	(h)	5	1	74	170	0.50	53.2
	(i)	5	1	124	170	0.50	46.7
	(j)	5	1	149	85	0.50	46.2
	(k)	5	1	124	170	1.75	45.5
	(l)	5	1	173	85	0.50	44.4
	(m)	5	1	149	170	0.50	44.2
	(n)	5	1	198	85	0.50	43.1
	(o)	5	1	173	170	0.50	42.5
	(p)	5	1	198	170	0.50	43.1

* Note: Ambient temperature is 25 °C

Table 7: Heat Flow Dependency on Radiation from Heat Sink

ϵ_s	$Q_{\text{sink}}/Q_{\text{total}}$	$Q_{\text{conv}}/Q_{\text{total}}$	$Q_{\text{rad}}/Q_{\text{total}}$	$T_{\text{max}}(^{\circ}\text{C})$
0.8	86%	51%	49%	80.4
0.2	78%	77%	23%	91.9

where ϵ_s = emissivity of the heat sink surface

Q_{sink} = heat transferred to the heat sink from the component

Q_{conv} = heat transferred to the air stream via natural convection

Q_{rad} = heat transferred to the air stream via radiation


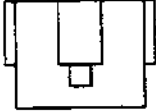
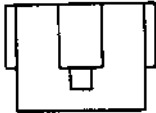
T_{max} = top surface temperature of the semiconductor chip

Table 8: Material Properties of the Second Mesh of the Navigator2

Material	k (W/m K)	ρ (kg/m ³)	C_p (J/kg K)	ρC_p (J/m ³ K)	u^{1n} (W/m ³)
stagnant air	0.05	1.1614	1007	1.17×10^3	0
plastic	0.50	-----	-----	1.70×10^6	0
Gap Pad*	0.50	-----	-----	1.70×10^6	0
aluminum	170	2500	860	2.15×10^6	0
PCB	0.20	100	800	8.00×10^4	0
Epson Card	120	1700	830	1.41×10^6	1.95×10^5
V.Reg.(0.5W)	32	800	770	6.16×10^5	1.26×10^5
V.Reg.(.75W)	32	800	770	6.16×10^5	1.89×10^5
V.Reg.(1.5W)	32	800	770	6.16×10^5	3.78×10^5

* Note: The ρC_p value for the plastic and Gap Pad is the average ρC_p value of the two materials. The conductivity (k) for the Gap Pad is being modelled as 0.5 W/m K instead of its actual conductivity (1.75 W/m K) to simulate the effect of contact resistance.

Effect of Heat Spreader Geometry & Convection Coefficient

<u>CASE</u>	<u>Material/POVVER</u>	<u>Conv. Coef.</u> (W/m ² °C)	<u>T_{max}</u>
A 	al-ox, 3.0 W	5 outside/stagnant inside	48.6
B 	al-ox, 3.0 W	5 outside/stagnant inside	51.4
C 	al-ox, 3.0W	5 inside/5 outside	47.4

Effect of Material Choice and Power Level

CASE	Material/ POWER	Conv. Coef. (W/m ² »c)	$L_{s,at} - T_{nmfT}$
A	al-ox. 3.0W	5 outside/stagnant inside	26.4 (2.9)
B	al-ox, 1.0W	5 outside/stagnant inside	9.1 (4.14)
C	al-ox, 0.2W	5 outside/stagnant inside	2.2
(1.82)			
D	Nylon, 3.0W	5 outside/stagnant inside	48.2 (2.9)
E	nylon, LOW	5 outside/stagnant inside	16.6 (4.15)
F	nylon. 0.2W	5 outside/ stagnant inside	4.0

f a b l e 11

Effects of Heat Spreaders and Air Channels

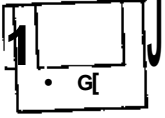


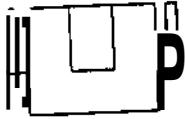
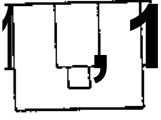
CASE	Material/POWER	Conv^hC_{ff}fiL (W/m² °C)	T_{max}
A	 al-ox, 3.0 W	5 outside/stagnant inside	51.4
B	 al-ox, 3.0W	5 outside/no air channel	50.5
C	 al-ox, 3.0W	5 outside/no heat spreader /no air channel	62.2
D	 al-ox, 3.0W	5 outside/2 inside h.spr. /no air channel	50.7
E	 al-ox, 3.0W	5 outside/3 inside h.spr. 12 in air channel	49.3

Table 12: Thermal Resistance Values of "Cube" with Extended Heat Spreaders

$$R_{\text{SUB.COND}} = \frac{L_{\text{SUB}}}{k_{\text{SUB}} A_{\text{SUB}}} = 5.94 \frac{\text{K}}{\text{W}}$$

$$R_{\text{HSR.SUB.COND}} = \frac{L_{\text{HSR.SUB}}}{k_{\text{SUB}} A_{\text{HSR.SUB}}} = 6.58 \frac{\text{K}}{\text{W}}$$

$$R_{\text{SUB.CONV}} = \frac{1}{h A_{\text{SUB}}} = 6.35 \frac{\text{K}}{\text{W}}$$

$$R_{\text{HSR.COND}} = \frac{L_{\text{HSR}}}{k_{\text{HSR}} A_{\text{HSR}}} = 2.21 \frac{\text{K}}{\text{W}}$$

$$R_{\text{HSR.CONV}} = \frac{1}{h A_{\text{HSR}}} = 20.24 \frac{\text{K}}{\text{W}}$$

$$R_{\text{eq}} = 3.12 \frac{\text{K}}{\text{W}}$$

$$R_{\text{SUB}} = 9.47 \frac{\text{K}}{\text{W}}$$

$$R_{\text{HSR}} = 22.45 \frac{\text{K}}{\text{W}}$$

$$R_{\text{TOTAL}} = 6.66 \frac{\text{K}}{\text{W}}$$

Table 13: Data from Polyurethane-Aluminum "Cube" Simulations

Power Level (W)	Max. Temp. (C)
0.20	26.98
0.40	28.67
0.60	30.36
0.80	32.06
1.00	33.75
1.20	35.44
1.40	37.14
1.60	38.84
1.80	40.52
2.00	42.22
2.20	43.91
2.40	45.60
2.60	47.30
2.80	49.00
3.00	50.69

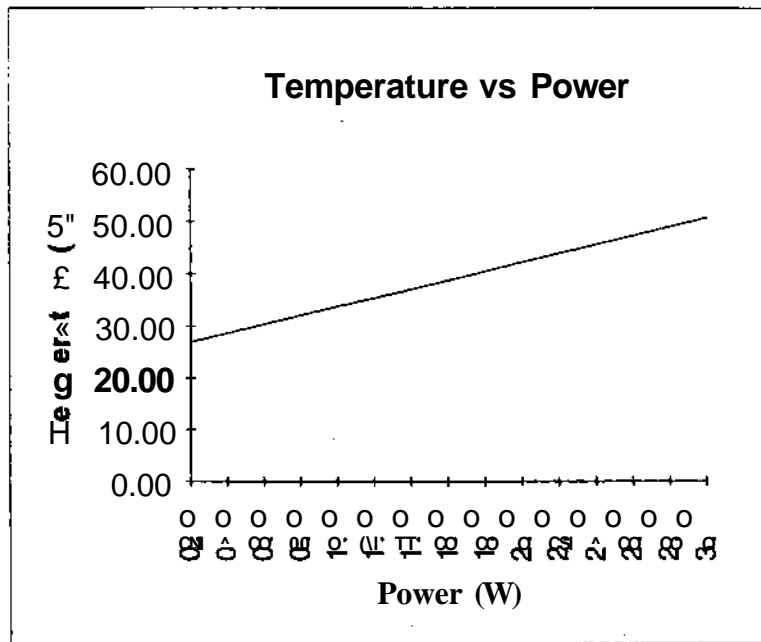


Table 14: Heat Flux Data for 3.0 W Poly-Al Ox "Cube with H.Spr. Only

$T_{\{max\}}$ (C)	$T_{\{sub\}}$ (C)	$T_{\{hsr\}}$ (C)	$T_{\{amb\}}$ (C)
50.69 [44.5]	39.94 [37.79]	45.06 [42.58]	25

$q_{\{sub\}}$ (W)	$q_{\{hsr\}}$ (W)	$q_{\{total\}}$ (W)	% heat thru heat spreader
2.35	0.99	3.34	0.296

Note: [] indicate Thermal Resistance Model values